Medium effects in high energy heavy-ion collisions

C. M. Ko and G. Q. Li

Cyclotron Institute and Physics Department

Texas A&M University, College Station, Texas 77843, USA

The change of hadron properties in dense matter based on various theoretical approaches are reviewed. Incorporating these medium effects in the relativistic transport model, which treats consistently the change of hadron masses and energies in dense matter via the scalar and vector fields, heavy-ion collisions at energies available from SIS/GSI, AGS/BNL, and SPS/CERN are studied. This model is seen to provide satisfactory explanations for the observed enhancement of kaon, antikaon, and antiproton yields as well as soft pions in the transverse direction from the SIS experiments. In the AGS heavy-ion experiments, it can account for the enhanced K^+/π^+ ratio, the difference in the slope parameters of the K^+ and K^- transverse kinetic energy spectra, and the lower apparent temperature of antiprotons than that of protons. This model also provides possible explanations for the observed enhancement of low-mass dileptons, phi mesons, and antilambdas in heavy-ion collisions at SPS energies. Furthermore, the change of hadron properties in hot dense matter leads to new signatures of the quark-gluon plasma to hadronic matter transition in future ultrarelativistic heavy-ion collisions at RHIC/BNL.

I. INTRODUCTION

An important feature of quantum chromodynamics (QCD) is its approximate $SU(3)_L \times SU(3)_R$ chiral symmetry as a result of small quark masses [1]. This symmetry is, however, spontaneously broken, leading to a finite quark condensate in vacuum, $\langle\bar{q}q\rangle_0 \approx \langle\bar{u}u\rangle_0 \approx \langle\bar{d}d\rangle_0$, as given by the Gell−Mann-Oaks-Renner relation,

$$m_\pi^2 f_\pi^2 = -2m_q\langle\bar{q}q\rangle_0. \tag{1}$$

In the above, $m_\pi \approx 138$ MeV and $f_\pi \approx a_\mu 93$ MeV are the pion mass and decay constant, respectively; and $m_q = (m_u + m_d)/2 \approx 5.5$ MeV is the average up and down quark masses. The quark condensate in vacuum thus has a value $\langle\bar{q}q\rangle_0 \approx -(245\,\mathrm{MeV})^3$.

As the density and/or temperature of a hadronic system increase, this spontaneously broken symmetry is expected to be partially restored, so the quark condensate would decrease with increasing density and/or temperature. At zero baryon chemical potential, the decrease of quark condensate with increasing temperature has been observed in lattice QCD simulations [2] as well as in calculations based on the chiral perturbation theory [3] and the interacting pion gas model [4]. At finite baryon density, model-independent studies using the Feynman-Hellmann theorem [5,6] have shown that the ratio of the quark condensate in medium to its value in vacuum is given by

$$\frac{\langle\bar{q}q\rangle_\rho}{\langle\bar{q}q\rangle_0} \approx 1 - \frac{\Sigma_{\pi N}}{f_\pi^2 m_\pi^2}\rho_N, \tag{2}$$

where ρ_N is the nuclear density and $\Sigma_{\pi N} \approx 45$ MeV is the πN sigma term. At normal nuclear matter density $\rho_0 \approx 0.16$ fm^{-3}, the condensate is seen to decrease already by $\approx 1/3$. Higher-order contributions to the quark condensate in nuclear matter due to nucleon-nucleon (NN) interactions have been studied using various models [6–11]. It is found that at normal nuclear matter density they change the leading-order result by only about 5% [9,11]. The decrease of quark condensate in medium may lead to reduced hadron masses as shown in QCD sum-rule studies [12,13]. The study of chiral symmetry breaking and partial restoration in hot dense matter is a topic of great current interest in nuclear physics [14–16].

In high energy heavy-ion collisions, theoretical simulations based on transport models have shown that a hot dense hadronic matter is formed in the initial stage of the collisions. This provides thus the possibility of studying the partial restoration of chiral symmetry through the changes of hadron properties in medium [17–19]. Unfortunately, the dynamics of heavy-ion collisions is very complex, involving a violent initial compression, which is then followed by a relatively slow expansion and finally reaches the freeze out when particle interactions become unimportant. The entire reaction typically lasts for about a few tens fm/c. The interesting physics of hadron in-medium properties and chiral symmetry restoration can only be studied for a few fm/c during the early part of the expansion stage when both the density and temperature of the hadronic matter are high. This stage of the collision can in principle be probed by detecting the emitted electromagnetic radiation such as the real and virtual (dilepton) photons. However, both are not easy to measure due to their small rates. Furthermore, they can also be produced from initial hard collisions and final hadron decays, and this makes it difficult to extract the signals from the hot dense matter. What are usually measured in heavy-ion experiments are instead the momentum distributions of hadrons, such as the nucleon, nuclear clusters, pion, kaon, etc., which are mostly ejected from the colliding system at freeze out. To infer what have happened in the initial hot dense matter from the final hadron phase space distributions requires thus a model that

can describe the whole collision process. Indeed, various transport models have been developed during the past ten years for this purpose. We shall review briefly the history of the development of transport models. We note that a number of good review articles are available on both relativistic and nonrelativistic transport models for heavy-ion collisions at various energies [20–27].

Since the reduced hadron masses in medium can be consistently included in the relativistic transport model [28–30] we shall concentrate mostly on the results obtained from this model. In the relativistic transport model, which is derived from the Walecka model [31,32], the effective hadron mass is connected to the scalar field while its energy is shifted by the vector potential. Because of dropping hadron masses due to the attractive scalar field, particle production is enhanced as a result of reduced threshold and increased phase space. Furthermore, the dense nuclear matter also provides a strong mean-field vector potential, which then affects the momentum distributions of hadrons. The relation of the Walecka model to the chiral effective field theory has recently been explored in Refs. [33–35]. The attractive scalar and repulsive vector potentials for a nucleon in nuclear matter have also been obtained in the Dirac-Brueckner-Hartree-Fock (DBHF) approach [36–41] as well as the QCD sum-rule studies [12,42–44].

For heavy-ion collisions at energies available from the SIS at GSI, the relativistic transport model gives a satisfactory explanation for the observed enhancement of kaon [45–48], antikaon [49,50], and antiproton yields [51,52] as well as low energy pions in the transverse direction [53–55]. Experiments on kaon flow have also provided important information on the kaon potential in dense matter [56,57]. Furthermore, the study of dilepton production from these collisions is expected to allow us to probe directly the in-medium properties of vector mesons in dense matter [58,59].

The relativistic transport model has also been used to describe the expansion stage of heavy-ion collisions at energies available from the AGS at BNL. It can account for the enhanced K^+/π^+ ratio [60], the difference between the slope parameters of the K^+ and K^- transverse mass spectra [61], and the lower apparent temperature of antiprotons than that of protons [62] as observed in experiments [63,64].

For the expansion stage of heavy-ion collisions at energies available from the SPS at CERN, it has been found that the relativistic transport model can explain quantitatively the observed enhancement of low-mass dileptons if one includes the decrease of vector meson masses in hot dense matter [65–69]. In a simplified hydrochemical model, medium effects also lead to enhanced production of phi mesons [70,71] and antilambdas [72,73] in these collisions.

The success of theoretical studies including the medium effects in explaining a large body of experimental data from high energy heavy-ion collisions thus provides the possible evidence for the partial restoration of chiral symmetry in hot dense matter formed in high energy heavy-ion collisions. The purpose of this article is to review the theoretical predictions for hadron properties in dense matter, the consistent incorporation of these medium effects in the relativistic transport model, and the observable consequences in heavy-ion collisions from SIS to SPS energies.

In Section II, hadron properties in dense matter are discussed using various theoretical approaches, such as the Walecka model, the DBHF approach, the QCD sum-rule approach, and the effective hadronic model. The relativistic transport model based on the nonlinear σ-ω model is then described in Section III, together with a brief review of the development of transport models. In Section IV, the results obtained from the relativistic transport model for particle production and flow in heavy-ion collisions at SIS energies, the strangeness enhancement in heavy-ion collisions at AGS and SPS energies, and dilepton production in heavy-ion collisions are then presented and compared with the experimental data. The relevance of these experimental observables as the probes of hadron properties in dense matter is emphasized. A summary and outlook is then given in Section V.

II. HADRONS IN DENSE MATTER

Theoretically, lattice QCD simulations should provide us with the most reliable information about the temperature and/or density dependence of hadron properties. Currently, these simulations can be carried out only for finite temperature systems with zero baryon chemical potential. Furthermore, the quenched approximation is usually introduced for quarks, so their dynamical role is only crudely included. From the hadronic correlation functions at large spatial separations the hadron screening masses have been obtained in the lattice QCD [74–76]. In a recent paper, Boyd *et al* [76] have shown that, up to about $0.92T_c$, where T_c is the critical temperature for the quark-gluon to hadronic matter phase transition, there is no significant change of the rho-meson screening mass. They have also found that the quark condensate does not change very much until one is extremely close to the critical temperature. This is in contrast with the result from chiral perturbation theory which shows a more appreciable decrease of the quark condensate with temperature [3]. Therefore, the study of hadron properties in dense nuclear matter at present time has to rely on theoretical models. In this section, we shall review some of these approaches. In particular, the properties of baryons (mainly nucleon), pseudoscalar mesons (mainly pion and kaon), and vector mesons (mainly rho, omega, and phi mesons) will be discussed.

A. baryons

A simple model for nuclear matter at high density is the Walecka model, also known as the quantum hadrodynamics (QHD-I) or linear σ-ω model, in which nucleons interact with each other through the exchange of a scalar sigma and a vector omega meson [31,32]. The sigma meson gives rise to an intermediate-range attraction while the omega exchange leads to a short-range repulsion, both are the essential properties of nuclear force. In this phenomenological model, the nucleon mass is reduced by the attractive scalar interaction, while its energy is shifted by the repulsive vector interaction. The parameters in this model are adjusted to fit the nuclear matter properties at saturation density using the mean-field approximation.

This model gives, however, too small a nucleon effective mass and too large a compression modulus at saturation density compared to what are known empirically. To correct for these deficiencies, self interactions of cubic and quartic forms have been introduced for the scalar field [77,78]. The Lagrangian for this nonlinear σ-ω model is given by

$$\begin{aligned}\mathcal{L} &= \bar{N}[\gamma_\mu(i\partial^\mu - g_\omega\omega^\mu) - (m_N - g_\sigma N)]N + \frac{1}{2}(\partial_\mu\sigma\phi\partial^\mu\sigma - m_\sigma^2\sigma^2) - \frac{1}{3}b\sigma^3 - \frac{1}{4}c\sigma^4 \\ &\quad - \frac{1}{4}(\partial_\mu\omega_\nu - \partial_\nu\omega_\mu)(\partial^\mu\omega^\nu - \partial^\nu\omega^\mu) + \frac{1}{2}m_\omega^2\omega_\mu\omega^\mu, \end{aligned} \tag{3}$$

where N is the nucleon field with mass m_N, while σ and ω_μ are the fields for the scalar and vector mesons with mass m_σ and m_ω, respectively. The parameters b and c determine the strength of scalar field self-interaction. With $b = c = 0$ the nonlinear σ-ω model reduces to the original Walecka model. The coupling constants between a nucleon and the scalar and vector fields are denoted by g_σ and g_ω, respectively. In a static nuclear matter, meson fields in the mean-field approximation become constants and are independent of the spatial coordinates. Furthermore, the vector field has a nonvanishing value only in its time-like component due to translational invariance in infinite nuclear

matter. The equation of motion for a nucleon with momentum $\mathbf{p}$ in a nuclear matter of density ρ_N is then given by the Dirac equation

$$(\boldsymbol{\alpha}\cdot\mathbf{p}+\beta m_N^*)N=\epsilon^*(\mathbf{p})N, \tag{4}$$

where the nucleon effective mass is related to the scalar potential $\Sigma_S=-g_\sigma\langle\sigma\rangle$, i.e.,

$$m_N^*=m_N+\Sigma_S, \tag{5}$$

and its energy is shifted by the vector potential $\Sigma_V^0=\frac{g_\omega^2}{m_\omega^2}\rho_N$, i.e.,

$$\epsilon^*=(m_N^{*2}+\mathbf{p}^2)^{1/2}+\Sigma_V^0. \tag{6}$$

While the vector potential is simply proportional to the nuclear density ρ_N, the scalar potential depends on the scalar density ρ_S via the following self-consistent equation, obtained by minimizing the energy,

$$m_\sigma^2\langle\sigma\rangle+b\langle\sigma\rangle^2+c\langle\sigma\rangle^3=g_\sigma\rho_S. \tag{7}$$

Table I Parameters of the nonlinear σ-ω model corresponding to the soft and stiff equations of state and the nuclear matter properties at the saturation density $\rho_0=0.16$ fm^{-3}.

	$C_\sigma=\frac{g_\sigma m_N}{m_\sigma}$	$C_\omega=\frac{g_\omega m_N}{m_\omega}$	$B=\frac{b}{g_\sigma^3 m_N}$	$C=\frac{c}{g_\sigma^4}$	$\frac{\mathcal{E}}{A}$ (MeV)	$\frac{m_N^*}{m_N}$	K (MeV)
soft	13.95	8.498	0.0199	-0.00296	-15.96	0.83	200.0
stiff	15.94	12.92	8.0×10^{-4}	2.26×10^{-3}	-15.96	0.68	380.0

The four parameters in the nonlinear σ-ω model are determined by the nuclear matter saturation density (ρ_0=0.16 fm^{-3}), binding energy (B=15.96 MeV), compression modulus (K), and the nucleon effective mass (m^*). In this review, only two sets of parameters, corresponding to the soft and stiff equations of state (EOS), are considered. At ρ_0, the soft EOS corresponds to $m_N^*/m_N=0.83$ and K=200 MeV, while the stiff EOS has $m_N^*/m_N=0.68$ and K=380 MeV. The corresponding parameters are listed in Table 1. The two nuclear equations of state, together with the nucleon effective mass, are shown in Fig. 1 by solid curves. Both the soft and the stiff equation of state in this relativistic formulation are very close to that from the Skyrme interaction [24] shown in the right panel of Fig. 1 by dotted curves.

It is worthy to mention that in the literature the expression 'effective mass' has been used to denote different quantities. A nice clarification of the relationship between these various quantities can be found in Ref. [79]. In nonrelativistic models, the nucleon effective mass is related to the nonlocality, or momentum dependence, of the single-particle potential. This quantity should be identified with the Lorentz mass [79] defined in terms of the Schrödinger-equivalent potential in relativistic models, rather than the Dirac mass defined in terms of the scalar potential as in Eq. (5).

Extensions of the Walecka-type model from zero to finite temperature have been studied in Refs. [80–82]. It is found that at finite density the nucleon effective mass first increases slightly at low temperature and then decreases

rapidly at high temperature. A similar temperature dependence of the constituent quark mass has been found in studies based on the Nambu−Jona-Lasinio model [83].

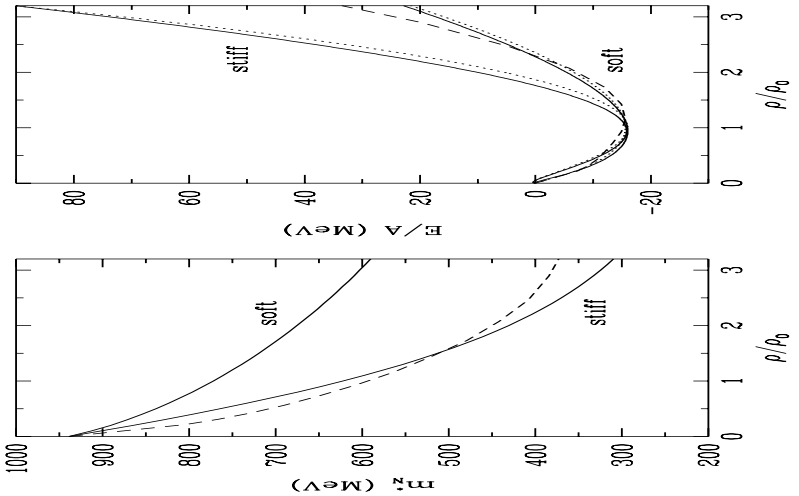

Fig. 1

Fig. 1 Left panel: The nucleon effective mass in medium. Solid and dashed curves are from the nonlinear σ-ω model and DBHF theory, respectively. Right panel: Nuclear equation of state. Dotted curves are from the Skyrme interaction.

A more microscopic approach to nucleon properties in nuclear matter is provided by the DBHF calculation [37–41] using, e.g., the Bonn one-boson-exchange potential [36,37]. As in conventional Brueckner approach, the basic quantity in DBHF approach is the G-matrix which satisfies the in-medium Thompson equation [37,40,41],

$$G(\mathbf{q}',\mathbf{q};\mathbf{P}) = V(\mathbf{q}',\mathbf{q}) + \int \frac{d^3k}{(2\pi)^3} V(\mathbf{q}',\mathbf{k}) \frac{m_N^{*2}}{E^{*2}_{\mathbf{P}/\mathbf{2}+\mathbf{k}}} \frac{Q(\mathbf{k},\mathbf{P})}{2E^*_{\mathbf{P}/2+\mathbf{q}} - 2E^*_{\mathbf{P}/2+\mathbf{k}}} G(\mathbf{k},\mathbf{q};\mathbf{P}), \tag{8}$$

with $E^*_{\mathbf{k}} = (m_N^{*2} + \mathbf{k}^2)^{1/2}$. The momenta $\mathbf{P}$ and $\mathbf{q}$ denote, respectively, the center-of-mass and the relative momentum of two interacting nucleons. The kernel of this integral equation is given by the sum of the one-meson-exchange amplitudes from six nonstrange bosons ($\pi, \sigma, \rho, \omega, \eta, \delta$). A form factor of monopole type is introduced at each meson-nucleon vertex to take into account the short-range dynamics due to quarks and gluons. The G-matrix becomes density-dependent through the Pauli projection operator Q and the scalar field Σ_S, which appears in m_N^* as shown by Eq. (5).

The Dirac equation and the in-medium Thompson equation are then solved self-consistently to determine the G-matrix, from which the nuclear matter properties can be derived. For example, the nuclear equation of state, or the energy-per-nucleon, is given by

$$\frac{\mathcal{E}}{A} = \frac{1}{A} \sum_{i \le k_F} \frac{m_N m_N^* + \mathbf{p}_i^2}{E_i^*} + \frac{1}{2A} \sum_{i,j \le k_F} \frac{m_N^{*2}}{E_i^* E_j^*} \langle ij|G|ij - ji\rangle - m_N, \tag{9}$$

where the nucleon bare mass has been subtracted out.

The G-matrix also allows one to determine the nucleon scalar and vector potentials in nuclear matter, i.e.,

$$\frac{m_N^*}{E_i^*}\Sigma_S + \Sigma_V^0 = \mathrm{Re}\sum_{j\le k_F}\frac{{m_N^*}^2}{E_i^* E_j^*}\langle ij|G|ij-ji\rangle. \tag{10}$$

The nuclear equation of state and the nucleon effective mass obtained from the DBHF calculation with the Bonn A potential are shown in Figs. 1 by dashed curves.

Nucleon properties in dense matter have also been studied in approaches based on the QCD. In the QCD sum-rule approach [5,12,42–44,84,85], hadron properties are related to a number of condensates, which are the vacuum expectation values of quark and gluon fields and describe the nonperturbative aspects of the QCD vacuum. The QCD sum rules have been quite successful in describing the hadron properties in free space, e.g, the nucleon mass is quantitatively reproduced in this approach [86–89]. The extension of QCD sum rules to hadrons in nuclear matter is achieved by using in-medium condensates. For a nucleon, it has been shown that the change of scalar quark condensate in medium leads to an attractive scalar potential which reduces its mass, while the change of vector quark condensate leads to a repulsive vector potential which shifts its energy [12,42–44]. The nucleon scalar and vector self-energies in this study are given, respectively, by

$$\begin{aligned}\Sigma_S &\approx -\frac{8\pi^2}{M_B^2}(\langle\bar{q}q\rangle_\rho - \langle\bar{q}q\rangle_0) \approx -\frac{8\pi^2}{M_B^2}\frac{\Sigma_{\pi N}}{m_u+m_d}\rho_N,\\ \Sigma_V &\approx \frac{64\pi^2}{3M_B^2}\langle q^+q\rangle_\rho = \frac{32\pi^2}{M_B^2}\rho_N,\end{aligned} \tag{11}$$

where the Borel mass M_B is an arbitrary parameter. With $M_B \approx m_N$, and $m_u + m_d \approx 11$ MeV, these self-energies have values which are similar to those determined from both the Walecka model and the DBHF approach.

Experimental evidences for these strong scalar and vector potentials have been inferred from the proton-nucleus scattering at intermediate energies [90] via the Dirac phenomenology [91,92] in which the Dirac equation with scalar and vector potentials is solved. The proton-nucleus scattering has also been successfully described using realistic NN interactions in the impulsive approximation [93,94] or the local density approximation [95].

In heavy-ion collisions at energies above the pion production threshold, baryon resonances can be produced. Transport model simulations have shown that in central heavy-ion collisions at incident energies around 1 GeV/nucleon, the baryon resonances to nucleon ratio can be as large as 0.2 [45]. This ratio approaches 1 when the incident energy is increased to about 10 GeV/nucleon at AGS [96,97]. The mean-field potentials for resonances are thus needed in transport models, and up to now have been assumed to be the same as those for a nucleon. This assumption for a delta particle seems to be supported by analyses of the pion-nucleus scattering data [98]. However, recent QCD sum-rule studies [99] have shown that the delta vector potential is considerably weaker than that for a nucleon, while its scalar potential is somewhat stronger. This would lead to a larger net attraction for a delta resonance than for a nucleon in nuclear medium.

Also of interest is the potentials for hyperons in nuclear matter. As for nucleon, most of the empirical information about hyperons in nuclear matter have been extracted from the structure of hypernuclei. The potential for the lambda particle is relatively well determined to be about -30 MeV [100]. The separation of this nonrelativistic potential into the scalar and vector potentials in the relativistic approach is, however, not without ambiguities [101].

The lambda potential in nuclear matter has also been studied using the DBHF approach [102]. The result ranges from -25 to -40 MeV, depending on the input boson-exchange models for the ΛN interaction. There have also been

various attempts to generalize the Walecka-type model from SU(2) to SU(3) to include the hyperon degrees of freedom [103–106]. In the naive SU(3) quark model, the hyperon potential is about 2/3 of the nucleon potential, as there are only two light quarks in a hyperon instead of three light quarks in a nucleon. Recently, hyperon properties in nuclear matter have also been studied using the QCD sum-rule approach. It has been found that both lambda scalar and vector potentials are significantly weaker than the prediction from the naive quark model [107], while those of the sigma hyperon are somewhat stronger and are close to the ones for the nucleon [108]. The accuracy of these findings are, however, limited by uncertainties in the nucleon strangeness content and certain in-medium four-quark condensates.

B. pseudoscalar mesons

Pseudoscalar mesons play a special role in nuclear physics. On the one hand, they are the Goldstone bosons of spontaneously broken chiral symmetry and are thus closely related to chiral symmetry restoration in nuclear medium. Furthermore, their small masses make the chiral perturbation theory applicable for low energy phenomena [109–112]. On the other hand, in heavy-ion collisions, pions are the most copiously produced particles; e.g., at SPS energies, the pion/nucleon ratio approaches 10 in midrapidity region. Knowledge on the properties of pseudoscalar mesons in medium is thus very important for understanding both chiral symmetry restoration and the dynamics of high energy heavy-ion collisions.

1. pion

Pion properties in dense matter have been a subject of extensive studies over many years [113]. The strong p-wave pion-nucleon interaction through the delta resonance is known to modify appreciably the pion dispersion relation at finite density [113–115]. In the delta-hole model, the pion dispersion relation in nuclear medium can be written as

$$\omega(\mathbf{k},\rho_B) = m_\pi^2 + \mathbf{k}^2 + \Pi(\omega,\mathbf{k}), \tag{12}$$

where the pion self-energy is given by

$$\Pi(\omega,\mathbf{k}) = \frac{\mathbf{k}^2\chi(\omega,\mathbf{k})}{1-g'\chi(\omega,\mathbf{k})}, \tag{13}$$

with $g' \approx 0.6$ being the Migdal parameter due to short-range correlations. The pion susceptibility χ is given by

$$\chi(\omega,\mathbf{k}) \approx \frac{8}{9}\Big(\frac{f_{\pi N\Delta}}{m_\pi}\Big)^2 \frac{\omega_R}{\omega^2-\omega_R^2}\exp\Big(-2\mathbf{k}^2/b^2\Big)\rho_N, \tag{14}$$

where $f_{\pi N\Delta} \approx 2$ is the pion-nucleon-delta coupling constant, $b \approx 7m_\pi$ is the range of the form factor, and $\omega_R \approx \frac{\mathbf{k}^2}{2m_\Delta} + m_\Delta - m_N$.

The pion dispersion relation obtained from this model is shown in Fig. 2. The pion branch in the lower part of the figure is seen to become softened, while the delta-hole branch in the upper part of the figure is stiffened. These results are, however, modified by the imaginary part of the pion self-energy due to the delta decay width and pion absorption [116–120]. As a result, the strength of the delta-hole branch is significantly reduced, and the peak in the spectral function is less shifted in energy than the pion branch obtained without the imaginary pion self-energy.

Pion properties in dense matter have also been studied using the chiral perturbation theory [121,122]. In effective chiral Lagrangians a pion has a negligible vector interaction with a nucleon. The s-wave πN scalar interaction, proportional to the πN sigma term $\Sigma_{\pi N}$, would lead to a reduction of the pion mass [121]. This effect is, however, almost completely canceled by the range term from the energy dependence of the πN scattering amplitude, so the net mean-field effects are quite small [123], and the pion mass is found to increase only slightly with increasing density. This is consistent with the results determined from the pionic atom data [113].

The Nambu−Jona-Lasinio model has also been used to study pion (or in general Goldstone boson) properties at both finite density and temperature [124,125]. In this model, pseudoscalar mesons are treated as quark-antiquark collective modes. Because of the finite scalar mean squared radius of a constituent quark, the s-wave πN attraction is found to be screened, leading to a slow increase of the pion mass with increasing density and/or temperature [125]. On the other hand, the pion mass is found to decrease slightly with temperature in an effective Lagrangian that includes its interactions in a pion gas via the rho and a_1 mesons [126].

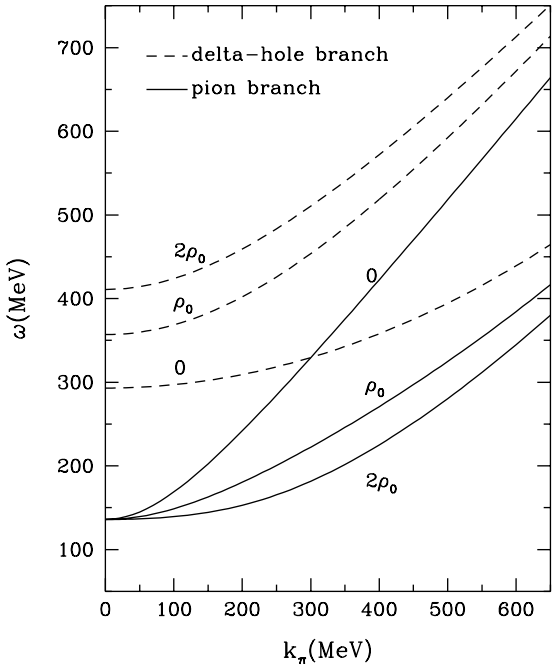

Fig. 2

Fig. 2 The pion dispersion relation from the delta-hole model. (From Ref. [115])

2. kaon

The study of kaon properties in dense matter has recently attracted a lot of attention as it is relevant for understanding not only the strangeness enhancement in heavy-ion collisions, which has been suggested as a possible signature of quark-gluon plasma formation in these reactions [127], but also the kaon condensation in neutron stars [128] and the possible formation of mini-black holes in galaxies [129].

The properties of kaon in dense matter were first studied in chiral Lagrangian by Kaplan and Nelson [130], and further pursued by many others [110–112,131–138]. The $SU(3)_L \times SU(3)_R$ nonlinear chiral Lagrangian used by Kaplan and Nelson is written as [130,134,136]

$$\begin{aligned}\mathcal{L} &= \frac{1}{4}f^2 \mathrm{Tr}\partial^\mu \Sigma \partial_\mu \Sigma^+ + \frac{1}{2}f^2\Lambda[\mathrm{Tr}M_q(\Sigma-1)+\mathrm{h.c.}] + \mathrm{Tr}\bar{B}(i\gamma^\mu\partial_\mu - m_B)B \\ &+ i\mathrm{Tr}\bar{B}\gamma^\mu[V_\mu, B] + D\mathrm{Tr}\bar{B}\gamma^\mu\gamma^5\{A_\mu, B\} + F\mathrm{Tr}\bar{B}\gamma^\mu\gamma^5[A_\mu, B] \\ &+ a_1\mathrm{Tr}\bar{B}(\xi M_q \xi + \mathrm{h.c.})B + a_2 \mathrm{Tr}\bar{B}B(\xi M_q\xi + \mathrm{h.c.}) \\ &+ a_3[\mathrm{Tr}M_q\Sigma + \mathrm{h.c.}]\mathrm{Tr}\bar{B}B. \end{aligned} \tag{15}$$

In the above, B is the baryon octet with a degenerate mass m_B, and

$$\Sigma = \exp(2i\pi/f), \quad \text{and} \quad \xi = \sqrt{\Sigma} = \exp(i\pi/f), \tag{16}$$

with π being the pseudoscalar meson octet. The pseudoscalar meson decay constants are equal in the $SU(3)_V$ limit and are denoted by $f = f_\pi \simeq 93$ MeV. The meson vector V_μ and axial vector A_μ currents are defined as

$$V_\mu = \frac{1}{2}(\xi^+\partial_\mu\xi + \xi\partial_\mu\xi^+) \quad \text{and} \quad A_\mu = \frac{i}{2}(\xi^+\partial_\mu\xi - \xi\partial_\mu\xi^+), \tag{17}$$

respectively. The current quark mass matrix is given by $M_q = \mathrm{diag}\{m_q, m_q, m_s\}$, if we neglect the small difference between the up and down quark masses.

Terms involving the axial vector current can be ignored as they have no effects on the kaon mass. Expanding Σ to order of $1/f^2$ and keeping explicitly only the kaon field, the first two terms in Eq. (15) can be written as

$$\partial^\mu \bar{K}\partial_\mu K - \Lambda(m_q + m_s)\bar{K}K + \cdots, \tag{18}$$

where

$$K = \begin{pmatrix} K^+ \\ K^0 \end{pmatrix} \quad \text{and} \quad \bar{K} = (K^- \quad \bar{K^0}), \tag{19}$$

and the ellipsis denotes terms containing other mesons.

Keeping explicitly only the nucleon and kaon, the third and fourth terms in Eq. (15) become

$$\bar{N}(i\gamma^\mu\partial_\mu - m_B)N - \frac{3i}{8f^2}\bar{N}\gamma^0 N\bar{K} \overset{\leftrightarrow}{\partial}_t K + \cdots, \tag{20}$$

where

$$N = \begin{pmatrix} p \\ n \end{pmatrix} \quad \text{and} \quad \bar{N} = (\bar{p} \quad \bar{n}), \tag{21}$$

and the ellipsis denotes terms involving other baryons and mesons.

The last three terms in Eq. (15) can be similarly worked out, and the results are

$$\begin{aligned}\mathrm{Tr}\bar{B}(\xi M_q\xi + \mathrm{h.c.})B &= 2m_q\bar{N}N - \frac{\bar{N}N}{2f^2}(m_q+m_s)\bar{K}K + \cdots, \\ \mathrm{Tr}\bar{B}B(\xi M_q\xi + \mathrm{h.c.}) &= 2m_s\bar{N}N - \frac{\bar{N}N}{f^2}(m_q+m_s)\bar{K}K + \cdots, \\ [\mathrm{Tr}M_q\Sigma + \mathrm{h.c.}]\mathrm{Tr}\bar{B}B &= 2(2m_q+m_s)\bar{N}N - \frac{2\bar{N}N}{f^2}(m_q+m_s)\bar{K}K + \cdots. \end{aligned} \tag{22}$$

Combining above expressions, one arrives at the following Lagrangian,

$$\begin{aligned}\mathcal{L} &= \bar{N}(i\gamma^\mu\partial_\mu - m_B)N + \partial^\mu\bar{K}\partial_\mu K - \Lambda(m_q+m_s)\bar{K}K \\ &- \frac{3i}{8f^2}\bar{N}\gamma^0 N\bar{K}\overset{\leftrightarrow}{\partial}_t K + [2m_q a_1 + 2m_s a_2 + 2(2m_q+m_s)a_3]\bar{N}N \\ &- \frac{\bar{N}N\bar{K}K}{2f^2}(m_q+m_s)(a_1+2a_2+4a_3) + \cdots. \end{aligned} \tag{23}$$

From this equation, one can identify the kaon mass by

$$m_K^2 = \Lambda(m_q+m_s) \tag{24}$$

and the nucleon mass by

$$m_N = m_B - 2[a_1 m_q + a_2 m_s + a_3(2m_q+m_s)]. \tag{25}$$

Also, the KN sigma term can be expressed as

$$\begin{aligned}\Sigma_{KN} &\equiv \frac{1}{2}(m_q+m_s)\langle N|\bar{u}u+\bar{s}s|N\rangle \\ &= \frac{1}{2}(m_q+m_s)\Big[\frac{1}{2}\frac{\partial m_N}{\partial m_q} + \frac{\partial m_N}{\partial m_s}\Big] \\ &= -\frac{1}{2}(m_q+m_s)(a_1+2a_2+4a_3). \end{aligned} \tag{26}$$

The second line in the above follows from explicit chiral symmetry breaking in the QCD Lagrangian, and the last step is obtained using Eq. (25). Then Eq. (23) can be rewritten as

$$\begin{aligned}\mathcal{L} &= \bar{N}(i\gamma^\mu\partial_\mu - m_N)N + \partial^\mu\bar{K}\partial_\mu K - (m_K^2 - \frac{\Sigma_{KN}}{f^2}\bar{N}N)\bar{K}K \\ &- \frac{3i}{8f^2}\bar{N}\gamma^0 N\bar{K}\overset{\leftrightarrow}{\partial}_t K + \cdots. \end{aligned} \tag{27}$$

The above Lagrangian does not describe properly the nuclear matter properties. In Ref. [134], an attempt has been made to combine this SU(3)$_L\times$SU(3)$_R$ chiral Lagrangian with the Walecka model [31,32] by allowing the nucleon to also couple with the phenomenological scalar (σ) and vector (ω) fields so that the saturation properties of nuclear matter can be obtained in mean-field level. Possible justifications of this approach have been further studied in Ref. [139] based on the chiral perturbation theory. Following this approach, one modifies Eq. (27) to

$$\begin{aligned}\mathcal{L} &= \bar{N}(i\gamma^\mu\partial_\mu - m_N + g_\sigma\sigma)N - g_\omega\bar{N}\gamma^\mu N\omega_\mu + \mathcal{L}_0(\sigma,\omega_\mu) \\ &+ \partial^\mu\bar{K}\partial_\mu K - (m_K^2 - \frac{\Sigma_{KN}}{f^2}\bar{N}N)\bar{K}K - \frac{3i}{8f^2}\bar{N}\gamma^0 N\bar{K}\overset{\leftrightarrow}{\partial}_t K + \cdots. \end{aligned} \tag{28}$$

In the above, $\mathcal{L}_0$ contains the kinetic and mass terms of the σ and ω fields as well as possible cubic and quartic σ self-interaction terms.

From the Euler-Lagrange equation and using the mean-field approximation for the nucleon field, i.e., replacing $\langle\bar{N}\gamma^0 N\rangle$ by the nuclear density ρ_N and $\langle\bar{N}N\rangle$ by the scalar density ρ_S, one obtains the following Klein-Gordon equation for a kaon in nuclear medium,

$$\Big[\partial_\mu\partial^\mu + \frac{3i}{4f^2}\rho_N\partial_t + \big(m_K^2 - \frac{\Sigma_{KN}}{f^2}\rho_S\big)\Big]K = 0. \tag{29}$$

The kaon dispersion relation in nuclear matter is then given by

$$\omega^2(\mathbf{k},\rho_B) = m_K^2 + \mathbf{k}^2 - \frac{\Sigma_{KN}}{f^2}\rho_S + \frac{3}{4}\frac{\omega}{f^2}\rho_N, \tag{30}$$

where $\mathbf{k}$ is the three-momentum of the kaon. The third term in the above equation is from the attractive scalar interaction due to explicit chiral symmetry breaking and depends on the kaon-nucleon sigma term Σ_{KN}. With a strangeness content of the nucleon, defined by $y = 2\langle N|\bar{s}s|N\rangle/\langle N|\bar{u}u + \bar{d}d|N\rangle \approx 0.1 - 0.2$ as normally used, its value is $370 < \Sigma_{KN} < 405$ MeV if one takes the strange quark to the light quark mass ratio to be $m_s/m \approx 29$. On the other hand, recent lattice gauge calculations [140,141] show that $y \approx 0.33$ which would give $\Sigma_{KN} \approx 450$ MeV. The last term in Eq. (30) is from the repulsive vector interaction and is proportional to the nuclear density ρ_N. For an antikaon this term becomes attractive due to G parity.

From the dispersion relation, the kaon energy in medium can be obtained, i.e.,

$$\omega(\mathbf{k},\rho_N) = \left[m_K^2 + \mathbf{k}^2 - \frac{\Sigma_{KN}}{f^2}\rho_S + \left(\frac{3}{8}\frac{\rho_N}{f^2}\right)^2\right]^{1/2} + \frac{3}{8}\frac{\rho_N}{f^2}. \tag{31}$$

Using the KFSR relation ($m_\rho = 2\sqrt{2}fg_\rho$) and the SU(3) relation ($g_\omega = 3g_\rho$) [142], the kaon vector potential in the last term can be written as $(1/3)(g_\omega/m_\omega)^2\rho_N$ which is just 1/3 of the nucleon vector potential. This can be understood in the constituent quark model as the kaon contains only one light quark as compared to three light quarks in a nucleon. Since an antikaon has one light antiquark, its vector potential becomes attractive, leading to a reduction of its energy in medium.

Corrections to the mean-field results of chiral Lagrangian have been studied in Refs. [110–112]. The term which contributes at the same order in chiral perturbation theory as the Kaplan-Nelson term is the energy-dependent range term, which can be included by multiplying the Kaplan-Nelson term by a factor $1 - 0.37\omega^2/m_K^2$ [34]. In Ref. [45], a smaller value of $\Sigma_{KN} \approx 350$ MeV has been used in evaluating the kaon scalar potential so that the effect of range term is effectively included. Also, the Nambu−Jona-Lasinio model has been used to estimate these corrections, and they are found to cancel off almost completely the attractive scalar potential [14]. One notes, however, that the former is based on a systematic expansion while the latter is model-dependent.

The in-medium kaon mass is normally given by the kaon energy at zero three-momentum. With $\Sigma_{KN} \approx 350$ MeV, the kaon mass increases by about 10 MeV at normal nuclear matter density as shown in Fig. 3. The antikaon mass is also shown and is seen to decrease with density as its vector potential is also attractive.

Because of baryon number conservation, vector potentials in the initial and final states of a hadron-hadron reaction are similar and can thus be neglected in estimating the threshold for particle production in medium. It is then sometimes useful to consider the kaon effective mass by including only effects due to the scalar field, i.e.,

$$m_K^* \approx m_K\left[1 - \frac{\Sigma_{KN}}{f^2 m_K^2}\rho_S\right]^{1/2}, \tag{32}$$

for both kaon and antikaon. In Ref. [136], the quadratic vector term, $\left(\frac{3}{8}\frac{\rho_B}{f^2}\right)^2$, in Eq. (31) was discarded based on the expectation that it would be cancelled by higher order terms not included in the calculation. Then, the kaon "effective" mass should involve only the scalar field, while the vector mean field shifts the kaon chemical potential or energy, as in Walecka mean-field theory.

From Eq. (31) one can define the kaon potential as the difference between its energies in the medium and in free space [56,143]. In the mean-field approximation this potential at normal nuclear matter density is about 10 MeV for a kaon at rest. This is smaller than what is expected from the impulse approximation using the kaon-nucleon (KN) scattering length in free space which gives about 30 MeV. The inclusion of higher-order terms [110–112] and possible scaling of the pion decay constant f in medium [34,144,145] would bring the chiral perturbation results in agreement with that obtained from the KN scattering length.

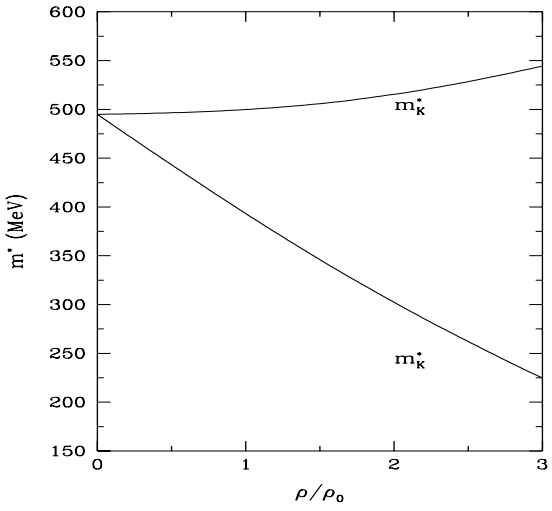

Fig. 3 Kaon and antikaon in-medium masses as functions of density from the mean-field approximation to the chiral Lagrangian.

Antikaon properties in nuclear matter deserve some further discussions. The possibility of K^- condensation in neutron stars has been the focus of many recent studies [110,146–149]. The isospin averaged K^-N scattering length is negative in free space [150], implying a repulsive K^- optical potential in the simple impulse approximation. However, a systematic analysis of the kaonic atom data shows that the K^- optical potential is deeply attractive, with a value of about 200± 20 MeV at normal nuclear matter density [151]. Unlike the kaon which interacts with nucleons relatively weakly so that the impulse approximation is reasonable, the antikaon interacts strongly with nucleons so we do not expect the impulse approximation to be reliable. The antikaon-nucleon ($\bar{K}N$) interaction at low-energy is strongly affected by the $\Lambda(1405)$ which is a quasi bound state of an antikaon and a nucleon in the isospin $I = 0$ channel and can decay into $\Sigma\pi$ channel [152,153]. Thus, in principle one needs to carry out a coupled-channel calculation for $\bar{K}N$, $\Lambda\pi$ and $\Sigma\pi$ including the effects of $\Lambda(1405)$ in both free space and in nuclear medium [152–157]. Because of Pauli blocking effects on the intermediate states, the possibility of forming a bound $\bar{K}N$ state ($\Lambda(1405)$) decreases with increasing density, leading to a dissociation of $\Lambda(1405)$ in nuclear medium. This induces a transition of the K^- potential from repulsion at very low densities to attraction at higher densities [153,156]. It was shown in Ref. [157], that, because of the diminishing role of $\Lambda(1405)$ in dense matter, the prediction for the kaon condensation threshold is relatively robust with respect to different treatments of $\Lambda(1405)$. Also, the strong attraction found in kaonic atoms can be understood in chiral perturbation theory if the possible scaling of the pion decay constant f in nuclear medium

is included [34,144,145].

C. vector mesons

Based on the restoration of scale invariance of QCD, Brown and Rho have argued that masses of nonstrange vector mesons would be reduced in dense matter [158,159]. This is supported by studies based on the QCD sum-rule approach [13], the effective hadronic model including $\bar{N}N$ vacuum polarization [160–162], and the quark-meson coupling model [163].

In the QCD sum-rule study of vector meson masses in nuclear medium, one considers the correlation function of a vector current,

$$\Pi_{\mu\nu}(q) = i \int e^{iqx} \langle T J_\mu(x) J_\nu(0) \rangle_\rho d^4x, \tag{33}$$

In nuclear medium, it can be written as

$$\begin{aligned} \Pi_{00} &= \mathbf{q}^2 \Pi_L, \\ \Pi_{ij} &= \left(\delta_{ij} - \frac{q_i q_j}{\mathbf{q}^2} \right) \Pi_T + \frac{q_i q_j \omega^2}{\mathbf{q}^2} \Pi_L, \end{aligned} \tag{34}$$

where Π_T and Π_L denote the transverse and longitudinal parts of the polarization tensor, respectively. At zero momentum, $\mathbf{q} = \mathbf{0}$, there is no distinction between the transverse and longitudinal directions, and Π_L is thus related to Π_T, i.e.,

$$\begin{aligned} \Pi_T &= (\omega^2 - \mathbf{q}^2) \Pi_L, \\ \Pi_L &= -\frac{1}{3\omega^2} g^{\mu\nu} \, \Pi_{\mu\nu}|_{\mathbf{q}\to\mathbf{0}} \, . \end{aligned} \tag{35}$$

In this case, only the longitudinal correlation function is needed.

For a rho meson, the current is taken to be

$$J_\mu^{(\rho)} = \frac{\bar{u}\gamma_\mu u - \bar{d}\gamma_\mu d}{2}. \tag{36}$$

For large Euclidean four momenta, $Q^2 (= -q^2 = -s) \to \infty$, $\Pi_L(Q^2)$ can be evaluated perturbatively by the operator product expansion (OPE) [88]. Including operators up to dimension 6, one has

$$\begin{aligned} \Pi_L(Q^2) = &-\frac{1}{8\pi^2} \left(1 + \frac{\alpha_s}{\pi} \right) \log \frac{Q^2}{Q_0^2} + \frac{m_q}{Q^4} \langle \bar{q} q \rangle_\rho + \frac{\alpha_s}{24\pi Q^4} \langle G_{\mu\nu} G^{\mu\nu} \rangle_\rho \\ &- \frac{\pi \alpha_s}{Q^6} \langle (\bar{q} \gamma_\mu \gamma_5 \lambda^a q)(\bar{q} \gamma^\mu \gamma_5 \lambda^a q) \rangle_\rho - \frac{2\pi\alpha_s}{9Q^6} \sum_{q'=u,d} \langle (\bar{q} \gamma_\mu \lambda^a q)(\bar{q'} \gamma^\mu \lambda^a q') \rangle_\rho. \end{aligned} \tag{37}$$

In the above, α_s is the QCD coupling constant while Q_0 is an arbitrary scale parameter. Both light quark masses and their expectation values are taken to be the same, i.e., $m_q = m_u \approx m_d$ and $\langle \bar{q} q \rangle_\rho = \langle \bar{u} u \rangle_\rho \approx \langle \bar{d} d \rangle_\rho$.

The imaginary part of the correlation function at $s > 0$ is related to the rho meson spectral function in medium and is normally parameterized phenomenologically by a contribution from the rho meson pole and a continuum, i.e.,

$$8\pi \mathrm{Im} \Pi_L(s) = F \delta(s - m_\rho^{*2}) + \left(1 + \frac{\alpha_s}{\pi} \right) \theta(s - s_0), \tag{38}$$

where F is a constant.

The theoretical side ($Q^2 > 0$) and the phenomenological side ($s > 0$) are related through the dispersion relation,

$$\mathrm{Re}\Pi_L(Q^2) = \frac{\mathrm{P}}{\pi}\int_0^\infty ds \frac{\mathrm{Im}\Pi_L(s)}{s+Q^2} + \text{ subtractions.} \tag{39}$$

From the above equation, the rho meson mass m_ρ^* and the continuum threshold s_0 can then be determined.

To suppress contributions from the higher order operators, one usually introduces the Borel transform defined by

$$L_{M_B} = \lim_{Q^2,n\to\infty;\, Q^2/n=M_B^2} \frac{1}{(n-1)!}(Q^2)^n \left(-\frac{d}{dQ^2}\right)^n, \tag{40}$$

where M_B is the Borel mass in Eq. (11). The Borel transform also removes the need for subtractions in the dispersion relation.

Carrying out the Borel transform of both sides of eq. (39) and taking the ratio of the resulting equation to its derivative with respect to $-1/M_B^2$, one obtains

$$\frac{m_\rho^*}{M_B^2} = \frac{(1+\frac{\alpha_s}{\pi})[1-(1+\frac{s_0}{M_B^2})e^{-s_0/M_B^2}] - \frac{8\pi^2 m_q}{M_B^4}\langle\bar{q}q\rangle_\rho - \frac{\alpha_s\pi}{3M_B^4}\langle G_{\mu\nu}G^{\mu\nu}\rangle_\rho + \frac{896\pi^3\alpha_s}{81M_B^6}\langle\bar{q}q\rangle_\rho^2}{(1+\frac{\alpha_s}{\pi})(1-e^{-s_0/M_B^2}) + \frac{8\pi^2 m_q}{M_B^4}\langle\bar{q}q\rangle_\rho + \frac{\alpha_s\pi}{3M_B^4}\langle G_{\mu\nu}G^{\mu\nu}\rangle_\rho - \frac{448\pi^3\alpha_s}{81M_B^6}\langle\bar{q}q\rangle_\rho^2}. \tag{41}$$

In deriving eq. (41), one has made use of the mean-field approximation,

$$\begin{aligned}\langle(\bar{q}\gamma_\mu\gamma_5\lambda^a q)(\bar{q}\gamma^\mu\gamma_5\lambda^a q)\rangle_\rho &\approx \frac{16}{9}\langle\bar{q}q\rangle_\rho^2,\\ \langle(\bar{q}\gamma_\mu\lambda^a q)(\bar{q'}\gamma^\mu\lambda^a q')\rangle_\rho &\approx -\frac{16}{9}\langle\bar{q}q\rangle_\rho^2\delta_{qq'}.\end{aligned} \tag{42}$$

Also, terms involving nonscalar operators due to lack of Lorentz invariance in a medium are not shown. Similar sum rules can be derived for the omega and phi meson masses, using the currents $J_\mu^{(\omega)} = (\bar{u}\gamma_\mu u + \bar{d}\gamma_\mu d)/2$ and $J_\mu^{(\phi)} = \bar{s}\gamma_\mu s$, respectively.

To determine the rho meson mass, one minimizes the sum rule, Eq. (41), with respect to the Borel mass M_B at an optimal s_0. In free space, using the commonly adopted values for the vacuum condensates ($\langle\bar{q}q\rangle_0 = -(245\,\mathrm{MeV})^3$, $\frac{\alpha_s}{\pi}\langle G_{\mu\nu}G^{\mu\nu}\rangle_0 = (330\,\mathrm{MeV})^4$), quark mass ($m_q = 5.5\,\mathrm{MeV}$), and QCD coupling constant ($\alpha_s = 0.3$), the empirical rho meson mass (776 MeV) can be reproduced with $s_0 \approx 1.77\,\mathrm{GeV}^2$ in the range of Borel masses $0.55 \le M_B^2 \le 0.75\,\mathrm{GeV}^2$.

In nuclear medium, vector meson masses depend on in-medium condensates. Because of small light quark masses, terms in Eq. (41) linear in quark condensates can be neglected. The results for ρ and ω mesons in nuclear medium thus depend on the density dependence of four-quark condensates. For phi meson, $\langle\bar{s}s\rangle_\rho$ dominates due to the relatively large strange quark mass $m_s \approx 100 \sim 200$ MeV, its in-medium mass thus depends on the nucleon strangeness content as $\langle\bar{s}s\rangle_\rho \approx \langle\bar{s}s\rangle_0 + \langle N|\bar{s}s|N\rangle\rho_N$, where $\langle\bar{s}s\rangle \approx -0.8\langle\bar{q}q\rangle_0$ is the strange quark condensate in vacuum. Based on the factorization assumption for the four-quark condensate, i.e., Eq. (42), and using a simple delta-function plus continuum ansatz for the vector meson spectral function as shown in Eq. (38), Hatsuda and Lee have obtained the following results for the in-medium vector meson masses [13],

$$\frac{m_{\rho,\omega}^*}{m_{\rho,\omega}} \approx 1 - 0.18(\rho_N/\rho_0), \tag{43}$$

and

$$\frac{m_\phi^*}{m_\phi} \approx 1 - 0.15y(\rho_N/\rho_0). \tag{44}$$

The density dependence of rho (omega) and phi meson masses is shown in Fig. 4, where the nucleon strangeness content is taken to be $y = 0.17$. It is seen that the rho (omega) meson mass decreases significantly with density due to a strong density dependence of the light quark condensate. Since the strange quark condensate does not change much in nuclear medium as a result of the small nucleon strangeness content, the phi meson mass thus shows a weaker density dependence. However, the phi meson mass would decrease substantially if the temperature is high so that many strange particles are present and reduce thus the strange quark condensate [164]. The temperature dependence of phi meson mass is shown in Fig. 5 and is seen to decrease significantly at high temperatures. We note that recent studies on phi meson mass at finite temperature using the hidden gauge theory [165,166] show a much smaller reduction than that from the QCD sum rules. This may be due to the incomplete treatment of vacuum effects in the latter approach as it is carried out only at the one-loop level.

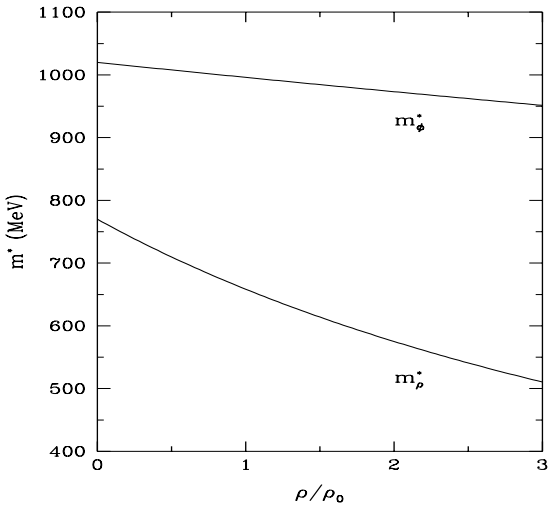

Fig. 4 Rho and phi meson masses as functions of density from QCD sum rules. (from Ref. [13])

A similar QCD sum-rule calculation of in-medium rho-meson mass has been carried out by Asakawa and Ko [167] using in the RHS of Eq. (39) a more realistic spectral function that is obtained by coupling the rho meson to pions via the vector dominance model and using the pion in-medium dispersion relation determined from the delta-hole model as discussed in Section II.B.1 [168,169]. A decrease of rho meson mass with increasing density as that of Ref. [13] has also been obtained. This is due to the stronger effect from reduced quark condensate in the presence of nucleons than that from the matter polarization.

Vector meson masses have also been studied using effective hadronic models [160–162]. Taking into account the change of $\bar{N}N$ vacuum polarization in medium as a result of reduced nucleon mass, the rho and omega meson masses have been found to decrease with density and temperature as in QCD sum-rule approach. If one includes only the matter effect, i.e., the polarization of the Fermi sea, the rho meson mass is seen to increase at high density. The inclusion of the vacuum effect, i.e., the polarization of the Dirac sea, however, brings the rho meson mass down in medium. The modification of the vacuum polarization in effective hadronic models is thus related to the change of quark condensate in medium in the QCD sum-rule approach. Since the nucleon is a composite particle, the large

effect of $\bar{N}N$ vacuum polarization has, however, been questioned in Ref. [170].

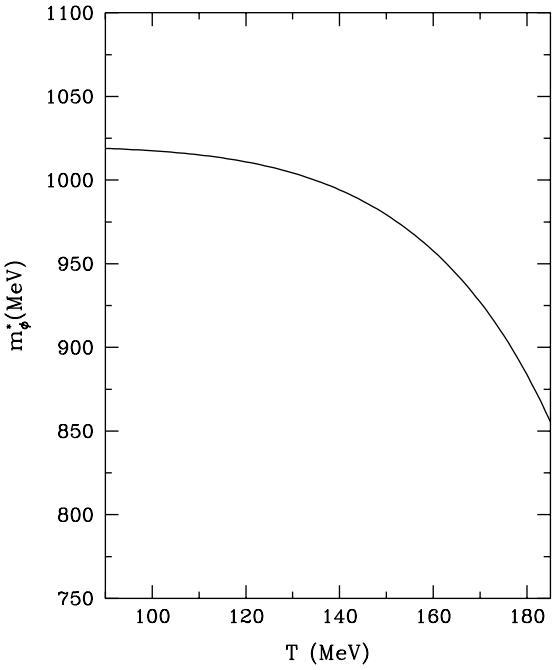

Fig. 5 Phi meson mass as a function of temperature from QCD sum rules. (from Ref. [164])

Experimentally, the quenching of the longitudinal response in quasielastic electron-nucleus scattering [171], and the enhancement of the K^+-nucleus scattering cross section [172,173] have been considered as indirect indication of the decrease of omega meson mass in nuclear medium. More direct observation of the vector meson mass in dense matter can be provided by the dilepton invariant mass spectrum from heavy-ion collisions. Since low-mass dileptons are mainly produced from pion-pion annihilation that proceeds through a rho meson, a change in the rho-meson mass in dense matter is expected to be reflected in the dilepton spectrum as a shift of the rho-meson peak to a lower mass [58]. Similarly, the in-medium properties of phi meson can be studied from the dilepton spectrum via kaon-antikaon annihilation.

III. THE RELATIVISTIC TRANSPORT MODEL

A. a brief review of the development of transport models

Heavy-ion collisions involve very complicated nonequilibrium dynamics and exhibit different features at different incident energies. At low energies, because of Pauli blocking of two-body collisions, a suitable approach is the mean-field theory, such as the time-dependent Hartree-Fock (TDHF) theory and its semiclassical approximation [174–178]. At high energies, the reaction dynamics at the initial stage is mainly governed by two-body collisions, so the mean-field can be safely neglected. Cascade-type models, in which heavy-ion reactions are visualized as a sequence of independent

two-body collisions, have been developed for this purpose, first for heavy-ion collisions at Bevalac energies [179,180], and recently for heavy-ion collisions at AGS [181] and SPS energies [182].

At energies between these two limits, and for the expansion stage of heavy-ion collisions at high energies, both the mean field and two-body collisions are important and need to be included in the model. There have been attempts to extend the TDHF approach to include the effects of two-body collisions. In this way, one obtains the extended time-dependent Hartree-Fock (ETDHF) equation, which were, however, found to be too complicated to be useful for heavy-ion collisions [183,184]. On the other hand, semiclassical approximations, which make it possible to treat heavy-ion collisions more efficiently, have been shown to give results that are close to that of TDHF [185]. This has thus led to the development of the well-known Boltzmann-Uehling-Uhlenbeck (BUU) equation, which is also known as the Vlasov-Uehling-Uhlenbeck (VUU), Landau-Vlasov (LV), and Boltzmann-Nordheim-Landau (BNL) equations [186–191]. The BUU equation includes simultaneously the effects of mean field, two-body collisions, and the Pauli principle. Its solution then gives the time evolution of the one-body phase space distribution function.

The BUU equation is usually solved by the test-particle method [192], in which the propagation of particles in the mean field (the Vlasov part) is given by the Hamilton's equation of motion, while two-body collisions (the Uehling-Uhlenbeck part) are treated by Monte-Carlo procedure. The introduction of test particles is necessary to remove numerical fluctuations associated with the evaluation of the mean field, but at the same time they also suppress correlations that are important for describing the instability and fragmentation of the system at low densities. A similar approach, the quantum molecular dynamics (QMD) [24,193,194], has thus been developed. In the QMD model each particle is represented by a Gaussian wave packet in both space and momentum. In this way, one can obtain a smooth mean field without introducing test particles (in other words, one test particle for one physical particle). The QMD model seems to provide a reasonable description of the nuclear fragmentation phenomena [24]. Similar but improved models, such as the fermionic molecular dynamics (FMD) [195] and the antisymmetrized molecular dynamics (AMD) [196,197], have also been developed.

The two important ingredients in these transport models, namely, the mean-field potential in the Hamilton's equation of motion and the in-medium cross sections for two-body scattering, are usually introduced separately. For example, the Skyrme parameterization [21,24] for the mean field and the Cugnon parameterization for the NN cross sections [21,198] are often used in transport models. Also, the momentum dependence of the nuclear optical potential has been introduced as it has been found to be important in describing the nucleon collective flow in heavy-ion collisions [199–202]. Since the mean field and in-medium two-body cross sections are related through the in-medium effective NN interactions (the G matrix), using separate parameterization inevitably introduces ambiguities in the transport models. There have been attempts to derive consistently the mean field and the in-medium two-body cross sections from the same underlying NN interactions [203–205].

Also, relativistic effects are expected to become important in heavy-ion collisions at high energies. Although relativistic kinematics have been incorporated in most transport models, the relativistic covariance, or the frame independence, of the transport model has only been addressed in the relativistic quantum molecular dynamics (RQMD) [182] and similar models [206] by the use of Hamiltonian dynamics that is constrained by Poincare invariants. The meson-exchange nature of NN interactions, by which the nucleon mean-field potential can be separated into different Lorentz components (e.g., scalar and vector potentials), has been included in the relativistic Boltzmann/Vlasov-Uehling-Uhlenbeck (RBUU/RVUU) approach [28–30]. The relativistic transport model allows one to investigate

consistently the medium effects on hadron properties through the change of the scalar and vector potentials. We shall discuss briefly in the next subsection the derivation of the relativistic transport model from Walecka-type models.

B. the relativistic transport model

Based on the Lagrangian of nonlinear σ-ω model, Eq. (3), in which the nuclear matter is treated as a system of interacting nucleons and mesons, a transport equation for the phase space distribution function of nucleons has been derived in Refs. [22,25,28,207–210] using the mean-field approximation..

An important quantity in these derivations is the nucleon Green's function, defined by

$$\begin{aligned} iG(x_1, x_{1'}) &= \langle |T[N(x_1)\bar{N}(x_{1'})]| \rangle \\ &= \theta(t_1 - t_{1'}) iG^{>}(x_1, x_{1'}) + \theta(t_{1'} - t_1) iG^{<}(x_1, x_{1'}), \end{aligned} \tag{45}$$

where $\langle \cdots \rangle$ denotes the expectation value in the nuclear many-body state and T is the time-ordering operator defined on a contour in the complex time plane [211,212]. It satisfies the following equation

$$(i\gamma_\mu \partial^\mu_{x_1} - m_N) G(x_1, x_{1'}) = \delta(x_1 - x_{1'}) + \int d^4u \Sigma(x_1, u) G(u, x_{1'}), \tag{46}$$

where Σ is the nucleon self-energy and can be evaluated via the perturbative expansion. The first-order nucleon self-energy is normally written as $\Sigma(x_1, x_2) \approx \Sigma_{HF}(x_1)\delta(x_1 - x_2)$ with

$$\Sigma_{HF}(x) = \Sigma_S + i\gamma_\mu \Sigma^\mu_V(x). \tag{47}$$

The scalar self-energy can be absorbed into the nucleon effective mass as in Eq. (5) while the vector self-energy leads to an effective momentum $p^*_\mu = p_\mu + \Sigma_{V\mu}$. In this limit, the nucleon Green's function satisfies the equation,

$$\{i\gamma_\mu [\partial^\mu_{x_1} - \Sigma^\mu_V(x_1)] - m^*_N(x_1)\} G^{<}(x_1, x_{1'}) = 0. \tag{48}$$

Introducing the Fourier transform of the nucleon Green's function

$$G^{<}(x, p^*) = \int d^4y e^{ipx} G^{<}(x + y/2, x - y/2), \tag{49}$$

then in local density and semi-classical approximations, it is related to the seven dimensional on-shell nucleon's phase-space distribution function $f(x, \mathbf{p}^*)$, i.e.,

$$\mathrm{Tr}[G^{<}(x, p^*)] = i16\pi\delta({p^*}^2 - {m^*_N}^2) m^*_N f(x, p^*). \tag{50}$$

From Eq. (48), a relativistic Vlasov equation follows and has the form

$$\{[\partial^\mu_x - (\partial^\mu_x \Sigma^\nu_v - \partial^\nu_x \Sigma^\mu_v)\partial^{p^*}_\nu] p^*_\mu + m^*_N (\partial^\mu_x m^*_N) \partial^{p^*}_\mu\} f(x, \mathbf{p}^*) = 0, \tag{51}$$

This equation can be more conveniently written as [213]

$$\frac{\partial}{\partial t} f + \mathbf{v} \cdot \nabla_x f - \nabla_x U \cdot \nabla_p f = 0, \tag{52}$$

where

$$\mathbf{v} = \mathbf{p}^*/E^*, \qquad U = E^* + (g_\omega/m_\omega)^2\rho_N, \tag{53}$$

with $E^* = ({\mathbf{p}^*}^2 + {m^*}^2)^{1/2}$.

In terms of the phase-space distribution function, the scalar and current densities in the local-density approximation can be expressed, respectively, as

$$\rho_s = 4\int \frac{d^3\mathbf{p}^*}{(2\pi)^3} f(x,\mathbf{p}^*) m^*/E^*, \quad \rho_\mu = 4\int \frac{d^3\mathbf{p}^*}{(2\pi)^3} f(x,\mathbf{p}^*) p^*_\mu/E^*. \tag{54}$$

In heavy-ion collisions the nucleon vector potential has both spatial-like and time-like components and are related to the nuclear current density ρ_μ.

The relativistic transport equation is solved by the test-particle method [192], so each nucleon is replaced by a collection of test particles. The one-body phase-space distribution function is then given by the distribution of these test particles in phase space. To solve the Vlasov equation is thus equivalent to solving the following classical equations of motion for all test particles,

$$\frac{d\mathbf{x}}{dt} = \mathbf{p}^*/E^*, \qquad \frac{d\mathbf{p}}{dt} = -\nabla_x U(x). \tag{55}$$

These equations of motion can be extended to other hadrons. For baryon resonances, they are the same as Eq. (55), as we have assumed that they have same mean-field potentials. For lambda and sigma hyperons, the corresponding mean-field potentials are taken to be 2/3 of those for the nucleon. The equations of motion for an antiproton are the same as those of the nucleon except that the sign of the vector potential is changed due to G parity. For a kaon, the equations of motion in the mean-field approximation to chiral Lagrangian [56] are obtained from Eq. (55) with $E^* = \left[m_K^2 + \mathbf{p}^2 - \frac{\Sigma_{KN}}{f^2}\rho_S + \left(\frac{3}{8}\frac{\rho_B}{f^2}\right)^2\right]^{1/2}$ and $U = \omega(\mathbf{p},\rho_B) - \omega_0(\mathbf{p})$, where $\omega(\mathbf{p},\rho_B)$ and $\omega_0(\mathbf{p})$ are the kaon dispersion relation in medium and in free space, respectively [143]. Again, the vector potential for an antikaon has an opposite sign from that of the kaon [49].

If one includes the second-order Born terms in the nucleon self-energy, then its imaginary part can be shown to lead to a collisional integral on the right hand side of the relativistic Vlasov equation [28,208], i.e.,

$$\begin{aligned} I_c = & \int \frac{d\mathbf{p}_2^*}{(2\pi)^3}\int \frac{d\mathbf{p}_3^*}{(2\pi)^3}\int d\Omega v \frac{d\sigma}{d\Omega}\delta^3(\mathbf{p}^* + \mathbf{p}_2^* - \mathbf{p}_3^* - \mathbf{p}_4^*) \\ & \cdot\{f(x,\mathbf{p}_3^*)f(x,\mathbf{p}_4^*)[1-f(x,\mathbf{p}^*)][1-f(x,\mathbf{p}_2^*)] - f(x,\mathbf{p}^*)f(x,\mathbf{p}_2^*)[1-f(x,\mathbf{p}_3^*)] \\ & \cdot[1-f(x,\mathbf{p}_4^*)]\}, \end{aligned} \tag{56}$$

where v is the relative velocity between the colliding particles and $\frac{d\sigma}{d\Omega}$ is the two-body NN differential scattering cross section calculated from meson exchanges. The factor $(1-f)$ takes into account the Pauli-blocking of fermions in the final state of a scattering.

For heavy-ion collisions at a few GeV/nucleon, nucleons, delta resonances, and pions are the most important degrees of freedom. As in normal BUU model [21], the isospin-averaged cross sections measured in free space [198] are used for the elastic ($NN \to NN$) and the delta excitation ($NN \to N\Delta$) process. The cross section for the inverse process $N\Delta \to NN$ is determined from the detailed balance relation [214]. Both the nucleon-delta ($N\Delta \to N\Delta$) and the delta-delta ($\Delta\Delta \to \Delta\Delta$) elastic collision are also allowed, and their cross sections are assumed to be the same as that for the nucleon-nucleon elastic scattering at the same center-of-mass energy.

When a delta is formed, its mass distribution is taken to be of the Breit-Wigner form

$$P(m_\Delta) = \frac{(\Gamma(q)/2)^2}{(m_\Delta - m_0)^2 + (\Gamma(q)/2)^2}, \tag{57}$$

where $m_0 = 1.232$ GeV and the momentum-dependent delta width [215], $\Gamma(q)$, is

$$\Gamma(q) = \frac{0.47q^3}{[1 + 0.6(q/m_\pi)^2]m_\pi^2}. \tag{58}$$

In the above, q is the pion momentum in the rest frame of a delta and is related to its mass m_Δ by $q = \sqrt{\left[m_\Delta^2 - (m_N + m_\pi)^2\right]\left[m_\Delta^2 - (m_N - m_\pi)^2\right]}/(2m_\Delta)$.

The collision between two baryons is treated in the same way as in cascade model [198]. A collision occurs when the distance between them is less than $\sqrt{\sigma/\pi}$ with σ being their interaction cross section. After the collision, directions of their momenta change in a statistical way according to the angular distribution. However, collisions are allowed only among particles in the same simulation but the mean nuclear density and current are computed with test particles from all simulations in the ensemble.

We note that a different treatment of two-body collisions has recently been introduced in Ref. [216]. In this approach, the collision between two particles is treated classically so that not only the angular momentum is conserved but also the reaction plane is preserved. Furthermore, only repulsive orbits are allowed in the collision due to the largely repulsive force in nucleon-nucleon scattering below 1 GeV/nucleon. An attempt to address the question of separating the nuclear interaction into a mean-field and a two-body collision part in nuclear collisions has recently been given in Ref. [217].

Pion production is included in the relativistic transport model through delta decay, i.e., $\Delta \to \pi N$, using the momentum-dependent delta decay width. The inverse reaction $\pi N \to \Delta$ is also included to take into account pion absorption [218–220]. In most transport models for pions, one does not include the pion potential so they propagate as free particles in nuclear medium. However, medium effects on pions are included in Ref. [53] by treating them as quasiparticles. It is found that softening of the pion dispersion relation might be responsible for the observed enhancement of low transverse energy pions in heavy-ion collisions at both Bevalac and SIS energies [54,55].

Because of their small production probability in hadron-hadron collisions, other particles, such as the kaon, antikaon, antiproton, and dilepton, are treated perturbatively, i.e., the collision dynamics is not affected by their presence [221,222]. These particles may also scatter with other hadrons. A kaon interacts only elastically with a baryon due to strangeness conservation, and the kaon-nucleon scattering cross section at low energies is about 10 mb in free space [223]. On the other hand, an antikaon, in addition to elastic scattering, can be absorbed by a nucleon through the strangeness-exchange process $\bar{K}N \to \pi Y$. These cross sections are also taken from Ref. [223]. Similarly, antibaryons can be annihilated by baryons, and their cross sections are taken from Ref. [224]. To include the final-state interactions of these particles, a perturbative test particle method has been introduced in [225]. In this method, one allows many particles to be produced in a hadron-hadron interaction. Each produced particle is then assigned a production probability, which is given by the ratio of its production cross section to the hadron-hadron total cross section. Their motions are then followed by solving the classical equations of motion. The collisions of these particles with nucleons are treated as usual except that their effects on nucleons are neglected, i.e., one does not allow the nucleon momenta to change in such collisions.

With reduced hadron masses in medium, the above cross sections should be modified as well. For nucleon-nucleon elastic scattering, the in-medium cross section has been evaluated in Ref. [226,227] in the DBHF approach using the

one-boson-exchange potentials. It is found that the magnitude of the cross section decreases with density and the differential cross section becomes more isotropic in medium. Experiments on proton-nucleus scattering [228–230] seem to be consistent with these predictions. The $NN \to N\Delta$ cross section in medium has been studied in Refs. [231–233] via the one-pion exchange model. Including the softening of the pion dispersion relation, its magnitude is found to increase with density. Recently, the same model has been used for evaluating the $\Delta\Delta \to \Delta\Delta$ cross section in medium [234]. Although the magnitude of the cross section is found to decrease with density, the density dependence is less pronounced than that of the nucleon-nucleon elastic cross section.

The $\Delta \leftrightarrow \pi N$ cross section in medium can be easily evaluated using in-medium hadron masses if one assumes that the cross section remains to be of the Breit-Wigner form. No theoretical studies have been carried out for the kaon-nucleon elastic cross section in medium. It is thus of interest to pursue such a study following the method of Ref. [227] by using the meson-exchange model of Ref. [235]. Similar calculations should also be done for the antikaon.

The production cross sections for kaon, antikaon, antiproton, and dilepton from hadron-hadron interactions in both free space and medium will be discussed below.

IV. MEDIUM EFFECTS IN HEAVY-ION COLLISIONS

In this section, results obtained from the relativistic transport model are presented and compared with the experimental data from heavy-ion collisions. In particular, discussions will be given for particle production and flow at SIS/GSI, strangeness enhancement at AGS/BNL and SPS/CERN, and dilepton production in heavy-ion collisions.

A. heavy-ion collisions at SIS energies

In heavy-ion collisions at SIS energies ($\sim$ 1 GeV/nucleon), the colliding system consists mainly of nucleons, delta resonances, and pions. In addition, particles with small production probability, such as the eta, kaon, antikaon, antiproton, and dilepton, can be created from baryon-baryon, meson-baryon, and meson-meson interactions during the course of the collisions. Since the threshold energies for eta, kaon, antikaon, and antiproton production in NN collisions in free space are, respectively, 1.26, 1.58, 2.5, and 5.6 GeV, their production in heavy-ion collisions at SIS energies is mostly below the production threshold in NN interactions in free space, and is known as 'subthreshold particle production'. Subthreshold particle production offers the possibility of exploring the extreme region of phase space, and thus may carry valuable information about the early, violent stage of heavy-ion collisions during which both density and temperature are high. In particular, the mean-field potential has been found to play an important role in subthreshold particle production [45,46,49,51,52,236–243]. This can be seen from Fig. 6, where we show the density dependence of the Q-value, which is defined by the difference between total hadron masses and potentials in the final and initial states, for the reaction $NN \to N\Lambda K$, $NN \to NNK\bar{K}$, and $NN \to NNN\bar{N}$. They are evaluated with the in-medium hadron masses and potentials discussed in Section II for the soft nuclear equation of state in Table I. It is seen that the Q-value increases slightly for the reaction $NN \to N\Lambda K$ but decreases appreciably for the reactions $NN \to NNK\bar{K}$ and $NN \to NNN\bar{N}$. In the ideal case that the scalar and vector potentials on a hadron in nuclear medium is determined by the sum of scalar and vector potentials on its constituent quarks, the Q-value for

the reaction $NN \to N\Lambda K$ is independent of density, while it is $2/3\Sigma_S$ and $2\Sigma_S$, respectively, below the values in free space for the reactions $NN \to NNK\bar{K}$ and $NN \to NNN\bar{N}$. At twice normal nuclear density, their values are -177 MeV and -530 MeV, respectively, which are slightly less than that shown in Fig. 6.

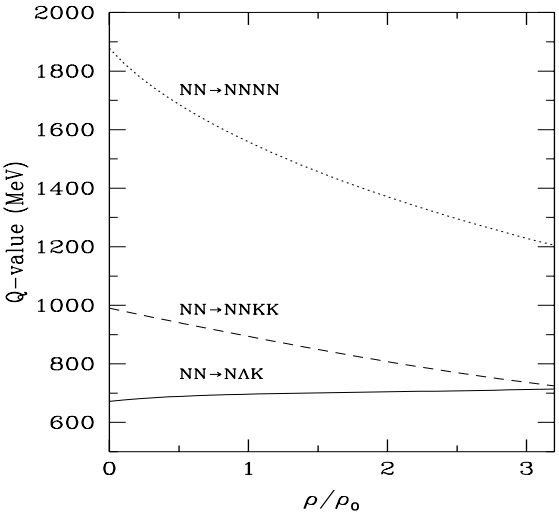

Fig. 6 The density dependence of the Q-value for the reactions $NN \to N\Lambda K$ (solid curve), $NN \to NNK\bar{K}$ (dashed curve), and $NN \to NNN\bar{N}$ (dotted curve).

1. subthreshold kaon production

The first experiment on kaon production in heavy-ion collisions was carried out at Bevalac in the eighties at incident energies around 2 GeV/nucleon [244,245]. These experiments had generated many theoretical studies based on both cascade and transport models [200,221,222,232,246–248]. Recently, there are new experiments on kaon production in heavy-ion collisions at incident energies around 1 GeV/nucleon by the KaoS collaboration at GSI [48]. This has led to a resurgence of theoretical studies based on both relativistic and nonrelativistic transport models [45–47,237–240]. The study of kaon production in heavy-ion collisions at subthreshold energies allows us to investigate the properties of the dense matter formed in the initial stage of the collisions. These include the nuclear equation of state, the role of baryon resonances, and the kaon in-medium properties.

To study the kaon production cross section in heavy-ion collisions, we need its production cross section in baryon-baryon interactions as the contribution from other processes is small. For example, it has been shown that in heavy-ion collisions the contribution to kaon production from pion-baryon interactions is only about 25% [249] while that due to many-body collisions is about 10% [250]. Randrup and Ko [221] have analyzed the available experimental data and proposed the following parameterization for the isospin-averaged kaon production cross section from the NN interaction in free space

$$\sigma_{NN\to BYK^+}(\sqrt{s}) \approx 36\ \frac{p_{\max}}{m_K}\ \mu\mathrm{b}, \tag{59}$$

where the kaon maximum momentum $p_{\rm max}$ is related to the NN center-of-mass energy $\sqrt{s}$ by $p_{\rm max} = \sqrt{\left[s-(m_B+m_Y+m_K)^2\right]\left[s-(m_B+m_Y-m_K)^2\right]/4s}$.

Kaon production cross sections from the nucleon-delta and delta-delta interactions have also been analyzed in Ref. [221] based mainly on isospin arguments. It has been found that the following scaling relations approximately hold,

$$\sigma_{N\Delta\to BYK^+}(\sqrt{s}) \approx \frac{3}{4}\sigma_{NN\to BYK^+}(\sqrt{s}),$$
$$\sigma_{\Delta\Delta\to BYK^+}(\sqrt{s}) \approx \frac{1}{2}\sigma_{NN\to BYK^+}(\sqrt{s}). \tag{60}$$

In addition to the total kaon production cross section, one also needs the kaon momentum distribution from baryon-baryon interaction in free space. This has been parameterized in Ref. [221] based on phase space considerations, i.e.,

$$\frac{d\sigma}{dp} \approx \sigma_{K^+}(\sqrt{s})\frac{12}{p_{\rm max}}\left(\frac{p}{p_{\rm max}}\right)^2\left(1-\frac{p}{p_{\rm max}}\right), \tag{61}$$

which reproduces reasonably the experimental data [221].

Using the one-pion plus one-kaon exchange model [251], it has been recently shown [47] that near kaon production threshold, where no experimental data are available, the cross sections in the Randrup-Ko parameterization and scaling ansatz are overestimated for the nucleon-nucleon interaction but underestimated for the nucleon-delta interaction. However, these discrepancy may be due to the neglect of final-state interactions, which have been shown to be important near the kaon production threshold [251].

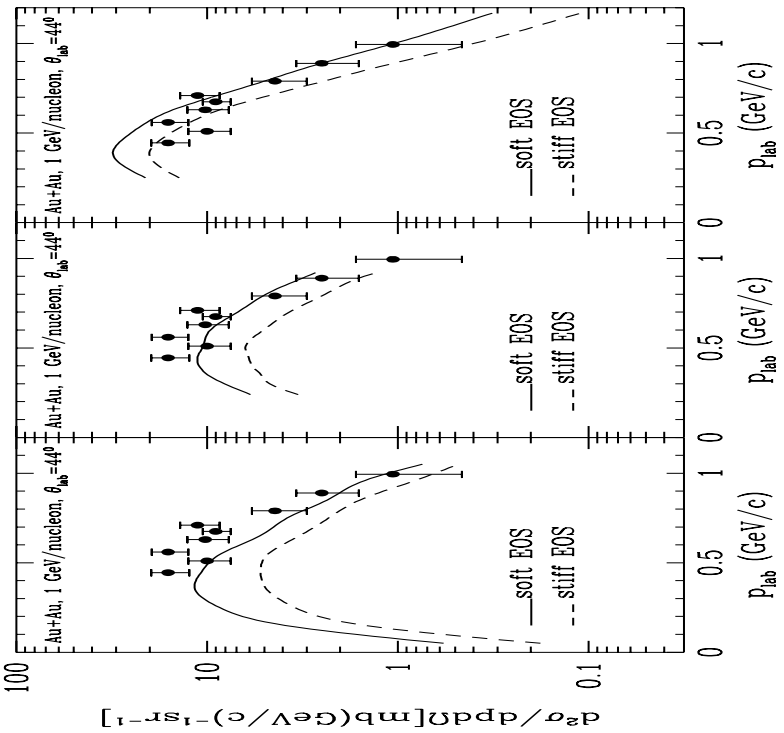

Fig. 7 Kaon momentum spectra from Au+Au collisions at 1 GeV/nucleon, obtained with the soft (solid) and stiff EOS (dashed), respectively. The left, middle, and right panels are from Refs. [46], [239], and [238], respectively. The experimental data from the KaoS collaboration [48] are also shown.

As first pointed out by Aichelin and Ko [222], the kaon yield from heavy-ion collisions at incident energies below the kaon production threshold in NN interaction in free space is sensitive to the nuclear equation of state at high densities. For Au+Au collisions at 1 GeV/nucleon, this dependence is shown in Fig. 7 in which the kaon momentum spectra obtained in three different calculations using the soft and the stiff equation of state are compared with experimental data from the KaoS collaboration [48]. The results in the left panel of Fig. 7 are from Ref. [46] based on the relativistic transport model including medium modifications of the kaon properties. In this calculation, the kaon production cross section in medium is obtained by using in-medium hadron masses to evaluate the $p_{\max}$ in Eq. (59). The results in the middle panel are from Ref. [239] based also on a relativistic transport model. The results in the right panel are from Ref. [238] using the nonrelativistic QMD model. Theoretical results from relativistic transport models with the soft EOS are in reasonable agreement with the experimental data, while that with the stiff EOS are below the data by about a factor of two. However, the results from the QMD calculation seem to favor a stiff nuclear equation of state. As explained below, the QMD calculation of Ref. [238] has overestimated the contribution from delta particle as they are only allowed to decay at freeze out. Thus, the KaoS data from Au+Au collisions at 1 GeV/nucleon seem to be consistent with a soft EOS.

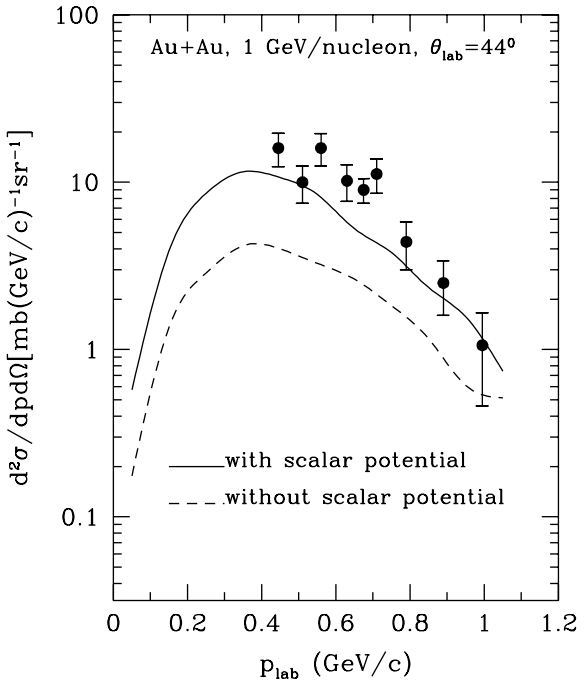

Fig. 8 Kaon momentum spectra from Au+Au collisions at 1 GeV/nucleon, obtained with (solid) and without (dashed) the kaon scalar potential. (from Ref. [45])

Subthreshold kaon production in heavy-ion collisions is also sensitive to the kaon scalar potential, and this is illustrated in Fig. 8. The solid and dashed curves correspond to results with and without kaon scalar potential, respectively. It is seen that without the attractive kaon scalar potential, the theoretical results are about a factor of 3-4 below the experimental data. This can be easily understood from Fig. 6 in terms of the Q-value for the reaction

$NN \to N\Lambda K$ in medium. At nuclear density $\rho = 2\rho_0$, where most kaons are produced in heavy-ion collisions, the Q-value is about 33 MeV above that in free space. Without the attractive kaon scalar potential, which is about 90 MeV, the Q-value is increased by the same amount. This increases the kaon production threshold and thus reduces its yield.

In the calculation of Ref. [239] based on the relativistic transport model, medium effects on kaons are not included so kaons are treated as free particles as in the nonrelativistic QMD calculation [237,238]. The results also agree with the experimental data and are thus comparable to that of Ref. [45], as shown in the middle panel of Fig. 7. Although the kaon mean-field potential is taken to be zero in Ref. [239], the scalar and vector potentials for the hyperon are taken to have the same strength as that for a nucleon, which is stronger than the hyperon mean-field potential used in Ref. [45], i.e., 2/3 of the nucleon mean-field potential. Thus, as far as the kaon production threshold is concerned, the treatment of Ref. [239] is approximately equivalent to Ref. [45] in which both kaon scalar and vector potentials are included.

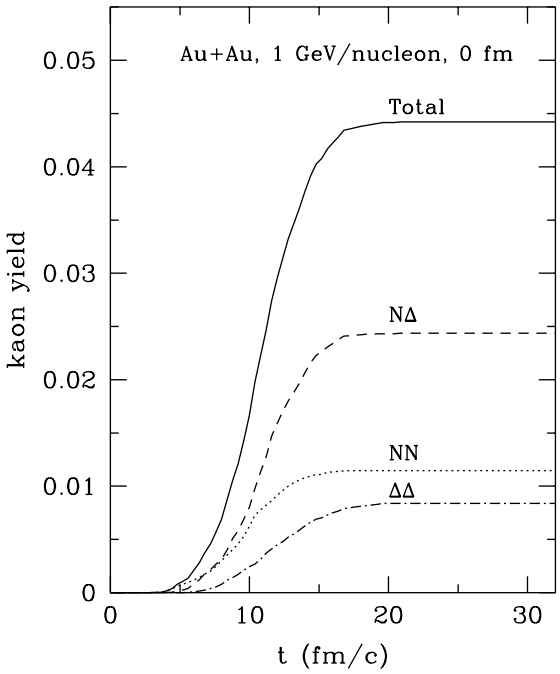

Fig. 9 Contributions to the total kaon production probability from the NN, NΔ and ΔΔ interactions in Au+Au collisions at 1 GeV/nucleon and impact parameter b=0 fm. (from Ref. [45])

Most kaons in heavy-ion collisions at subthreshold energies are produced from the two-step process in which a nucleon is first excited to a resonance and a kaon is then produced from the interaction of the resonance with another baryon. At incident energies around 1 GeV/nucleon, only the delta resonance is appreciably produced. Subthreshold kaon production can thus serve as a good probe of the properties of (delta) resonance matter. In Fig. 9, the total kaon production probability in Au+Au collisions at an incident energy of 1 GeV/nucleon and an impact parameter of b=0 fm from the relativistic transport model is separated into contributions from the nucleon-nucleon, the nucleon-

delta and the delta-delta interaction. It is seen that the contribution from the nucleon-delta interaction accounts for more than half of the total kaon yield, and the sum of contributions from the nucleon-delta and delta-delta interactions is about 75% of the total kaon yield. Contrary to that of Refs. [237,238], the contribution from the delta-delta interaction is slightly smaller than that from the nucleon-nucleon interaction. This is mainly due to following two reasons. First, in Refs. [237,238], deltas are allowed to decay only at final stage of the collision. This treatment certainly overestimates the contribution from the nucleon-delta and delta-delta interactions. Secondly, kaon production in Refs. [237,238] is calculated in the QMD with a Skyrme-type momentum-independent mean-field potential. It is well-known that introducing a momentum-dependence in the nucleon mean-field potential, which is automatically included in the relativistic transport model [252], reduces the number of two-body collisions and hence the delta abundance, thus leading to a smaller contribution from the delta-delta interaction as compared to the case with a momentum-independent mean-field potential.

Although the interaction of a kaon with a nucleon is relatively weak as compared to other hadrons, they are still scattered by baryons in the dense medium [225,253]. Furthermore, kaons propagate in both scalar and vector mean-field potentials. These final-state interactions change the kaon momentum spectra but not its total yield, leading to an increase of both its yield and the slope of its spectra at large angles. Actually, final-state interactions help to bring the theoretical results at $\theta_{\rm lab} = 44^o$ in better agreement with the experimental data. Since final-state interactions increase the kaon yield at large angles, it would be of interest to have experimental data to test this prediction.

2. subthreshold antikaon production

Effects of the attractive scalar potential can be more clearly seen in antikaon production than in kaon production as it leads to a significant reduction of the Q-value for the reaction $NN \to NNK^+K^-$ in nuclear medium as shown in Fig. 6. From the analysis of available experimental data, Zwermann and Schürmann [254] have proposed the following parameterization for the antikaon production cross section from nucleon-nucleon interaction in free space,

$$\frac{d\sigma}{dp} \approx 0.75 \left(\frac{p}{p_{\rm max}}\right)^2 \left(1 - \frac{p}{p_{\rm max}}\right)^2 \ {\rm mb/GeV}, \tag{62}$$

where $p_{\rm max} = \sqrt{[s-(2m+2m_K)^2](s-4m^2)/(4s)}$. It has been usually assumed that the same cross section is applicable for antikaon production from the delta-nucleon and the delta-delta interaction.

Including all final-state interactions (propagation in mean fields, elastic scattering, and absorption) for antikaons, the results from the relativistic transport model for the antikaon production cross section from ^{58}Ni+^{59}Ni collisions at 1.85 GeV/nucleon are shown in Fig. 10 [49]. The dashed curve gives the results using free kaon and antikaon masses, while the results with in-medium kaon and antikaon masses are shown by the solid curve. Also shown in the figure by solid circles are the experimental data from the SIS at GSI [50].

Using free kaon and antikaon masses, the theoretical results are about a factor of 5-10 smaller than the experimental values. The antikaon yield is enhanced by a factor of 4-5 when in-medium kaon and antikaon masses are used. The theoretical results are now in reasonable agreement with the experimental data, except at $p^{\bar{K}}_{lab}$=1.0 GeV/c where they are still below the data by about a factor of two. Including possible decrease of the pion decay constant in medium, which leads to a stronger reduction in antikaon mass, is expected to further increase the calculated antikaon yield.

Subthreshold antikaon production in heavy-ion collisions has also been measured earlier at Bevalac for Si+Si collisions at 1.55 and 2.1 GeV/nucleon [245]. Theoretical calculations using the QMD model without medium effects give results that are also smaller than the experimental data by about a factor of 3-4 [248,255]. Again, this discrepancy is likely explained by the modifications of kaon and antikaon masses in medium.

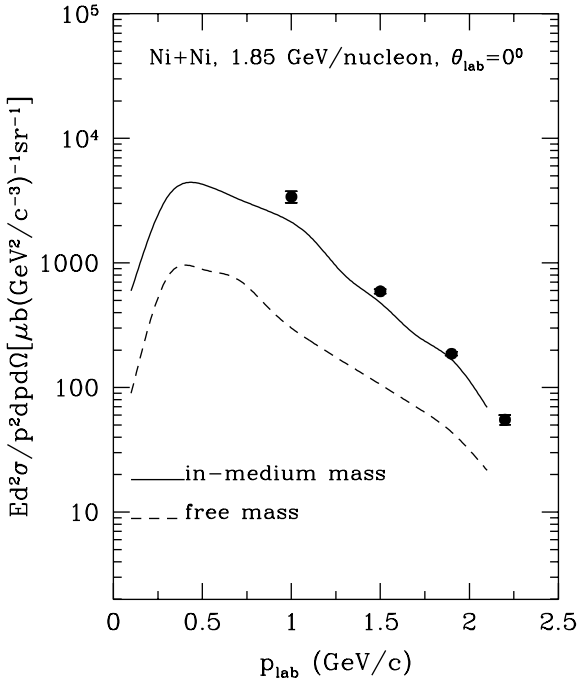

Fig. 10 Antikaon momentum spectra from Ni+Ni collisions at 1.85 GeV/nucleon, obtained with free (dashed) and in-medium (solid) kaon and antikaon masses. The experimental data from Ref. [50] are shown by solid circles. (from Ref. [49])

It should be noted that an antikaon can also be produced from the process $\pi Y \to \bar{K}N$ between a pion and a hyperon Y produced from the reaction $BB \to NYK$. However, with the cross section of Ref. [256] obtained from the K-matrix analysis of Ref. [223], it has been found that the antikaon yield from $\pi Y \to \bar{K}N$ in heavy-ion collisions is only about 25% of that from $BB \to NNK\bar{K}$. This is less than that from calculations based on the kinetic model [257] and the cascade model [258], where more than 50% of the antikaons are from this process. These earlier calculations are, however, less accurate than the one based on the transport model as they do not treat properly the collision dynamics and antikaon absorption. Similarly, antikaon production from $\pi B \to NK\bar{K}$ has been found to be much smaller than that from BB interactions. Furthermore, the reaction $NY \to NNK\bar{K}$ is unimportant due to the small cross section [256]. We note that these estimates were all based on calculations without including medium effects and need to be further investigated.

Antikaon production from ϕ decay could also be included in the transport model calculation. Unfortunately, the elementary ϕ production cross section in nucleon-nucleon interaction is only scarcely available at high beam momenta. At a beam momentum of 10.0 GeV/c, the ϕ production cross section is 1.0±0.1 μb [259] in proton-proton interaction.

This is to be compared with the antikaon production cross section of 33±16 μb at the same beam momentum [260]. Also, recent experiments at the AGS indicate that, at an incident energy of 14.6 GeV/c per nucleon, the ratio of ϕ to K^- in a Si+Au collision is about 12% [261]. We expect an even smaller ratio in heavy-ion collisions at beam energies of about 1-2 GeV/nucleon, and the contribution from phi decay to subthreshold antikaon production can thus be neglected [262].

3. subthreshold antiproton production

With a threshold at 5.6 GeV in nucleon-nucleon interaction in free space, antiproton production in nucleus-nucleus collisions at energies of a few GeV/nucleon is clearly the most extreme subthreshold process in particle production from heavy-ion collisions. The first observation of subthreshold antiproton production in proton-nucleus collisions dated back to the fifties [263] and sixties [264,265]. The experiments at the Bevalac [245] and the JINR [266] in the eighties provided the first evidence of subthreshold antiproton production in nucleus-nucleus collisions. Recently, new measurements of subthreshold antiproton production have been carried out at both KEK [267] and GSI [50].

The antiproton momentum spectrum in proton-proton interaction in free space has been parameterized as [263,264,268]

$$\frac{d\sigma}{dp} \approx \sigma_{\bar{p}}(\sqrt{s}) \frac{105}{8p_{\max}} \left(\frac{p}{p_{\max}}\right)^2 \left[1 - \left(\frac{p}{p_{\max}}\right)^2\right]^2, \tag{63}$$

where the maximum momentum of the antiproton, $p_{\max}$, is related to the available center-of-mass energy $\sqrt{s}$ of the proton pair by $p_{\max} = \sqrt{(s - 16m_N^2)(s - 4m_N^2)/4s}$.

This parameterization is based on phase space arguments and describes reasonably well the measured antiproton momentum spectrum in proton-proton collisions [263,264,268]. The total antiproton production cross section in Eq. (63) is fitted to the available experimental data, i.e.,

$$\sigma_{\bar{p}}(\sqrt{s}) \approx 0.012(\sqrt{s} - 4m_N)^{1.846} \text{ mb}. \tag{64}$$

The first investigation of subthreshold antiproton production using the transport model has been carried out by Batko *et al.* [269]. In this study, the $\Delta(1232)$ degree of freedom is included and is found to play an important role. Neglecting the antiproton mean field and assuming that 90% of the primordial antiprotons are absorbed, Batko *et al.* [269] have achieved a reasonable description of antiproton production in proton-nucleus collisions, but their results for nucleus-nucleus collisions are about a factor of five too small compared with the experimental data. A similar calculation has been carried out by Huang *et al.* [255] using the QMD. Again, the antiproton yield in nucleus-nucleus collisions is less than the experimental data by about the same factor as in Ref. [269]. In both calculations [255,269], antiproton annihilation is treated schematically, and the propagation as well as elastic scattering of antiprotons in medium are neglected.

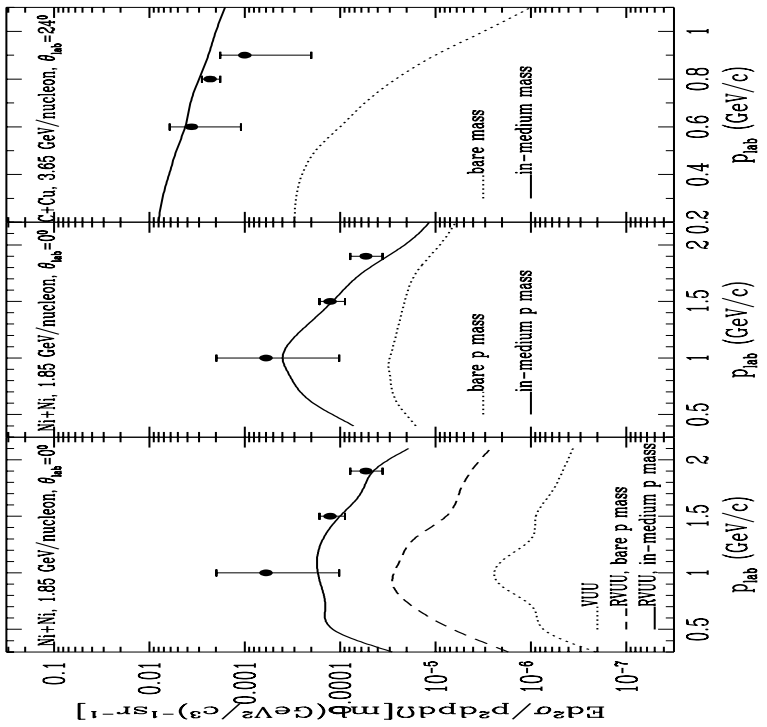

Fig. 11 Antiproton momentum spectra from Ni+Ni collisions at 1.85 GeV/nucleon, and C+Cu collisions at 3.85 GeV/nucleon. The left, middle, and right panels are from Refs. [52], [241], and [242], respectively. The experimental data from Ref. [50] for Ni+Ni collisions and from Ref. [266] for C+Cu collisions are shown by solid circles.

The importance of medium effects can be seen from the significant decrease of the Q-value shown in Fig. 6 for the reaction $NN \to NNN\bar{N}$ in nuclear medium as a result of the attractive scalar potential. This effect has been included in a number of studies based on transport models. In Fig. 11, theoretical results from these calculations for the antiproton differential cross section in Ni+Ni collisions at 1.85 GeV/nucleon and C+Cu collisions at 3.65 GeV/nucleon are compared with the experimental data from both GSI [50] and Dubna [266]. In the left panel, the results from Ref. [52] based on the relativistic transport model are shown. The antiproton mean-field potential is obtained from the nucleon one by G parity and is thus very attractive. It is indeed seen that the experimental data can only be accounted for if in-medium baryon masses (solid curve) are used. The results with dropping only the nucleon mass but not the antiproton mass are shown by the dashed curve and are a factor of 8 smaller. When free baryon masses are used in the calculation, the antiproton yield (dotted curve) is further reduced by a factor of 12. Overall, the antiproton production cross section is enhanced by about two orders of magnitude due to the reduction of baryon masses in medium. Similar results [51] have been obtained for antiproton production from Si+Si at 2.1 GeV/nucleon [245].

The results in the middle panel of Fig. 11 are from Ref. [241] based also on the relativistic transport model. The results shown by the solid curve for the case with an in-medium antiproton mass are in good agreement with the data, while that with a bare antiproton mass (but still an in-medium nucleon mass) are below the data by about a factor of 5-10. We note that the theoretical results of Refs. [52,241] agree with each other within a factor of two, and

the antiproton potential at normal nuclear matter density extracted from these calculations is in the range of -150 to -250 MeV.

The results in the right panel of Fig. 11 are from Ref. [242] based on the nonrelativistic QMD model. Medium effects on the produced nucleon and antinucleon masses are taken from the Nambu−Jona-Lasinio model. It is again seen that without medium effects the theoretical results are much below the experimental data. These studies thus show that in order to describe the antiproton data from heavy-ion collisions at subthreshold energies it is necessary to include the reduction of both nucleon and antinucleon masses in nuclear medium. Even at AGS energies, which are above the antiproton production threshold in NN interaction, a recent calculation using the RQMD shows that medium modifications of the antiproton properties are important for a quantitative description of the experimental data [270].

On the other hand, there have been suggestions based on schematic considerations that the contributions from quasi-coherent multi-particle collisions [268] and meson-meson interactions (e.g. $\rho\rho \to p\overline{p}$) [271] might be significant. More accurate estimates of these contributions using the transport model have not been done and are needed.

4. soft pions

Transport models have also been used to study pion production from heavy-ion collisions. Of particular interest is the experimental observation of enhanced low (transverse) momentum pions in these collisions at various energies [54,55,272,273]. Different mechanisms have been proposed to explain this phenomenon, including the collective flow [274], the resonance decay at freeze-out [220,275–277], the finite pion chemical potential at freeze-out [278,279], and the medium modifications of the pion dispersion relation [53,280–282]. In this subsection, we discuss mainly the results for heavy-ion collisions at Bevalac and SIS energies.

Several nonrelativistic BUU calculations have been carried out by different groups for the pion spectra from heavy-ion collisions at 1-2 GeV/nucleon [53,220,280,283]. The results of Ref. [53] for the pion kinetic energy spectra from La+La collisions at 1.35 GeV/nucleon are shown in the left panel of Fig. 12. The dashed histogram is obtained using the free-space pion dispersion relation, and for low energy pions it differs significantly from the experimental data shown by solid circles with error bars [54]. With a softened pion in-medium dispersion relation described in Section II.B.1., there is an enhancement of low energy pions as shown by the solid histogram. This enhancement is due to several mechanisms. From delta decays in dense medium, quasipions in the pion branch generally carry less energy than free pions. With their increased widths, it is more probable to form small mass deltas, so that more soft pions are created from the decay of these deltas. Also, as quasipions propagate from a more dense region to a less dense region, as most likely happened during heavy-ion collisions, their momenta should decrease since the p-wave interaction reduces. Enhanced soft pions are also seen in more recent experiments at SIS [55]. Calculations within transport models with a free pion dispersion relation fail to explain this enhancement [280,283]. A similar enhancement of low energy etas has also been observed [284], and this may again be due to the change of the eta dispersion relation in medium as a result of the $N^*(1535)$-hole polarization.

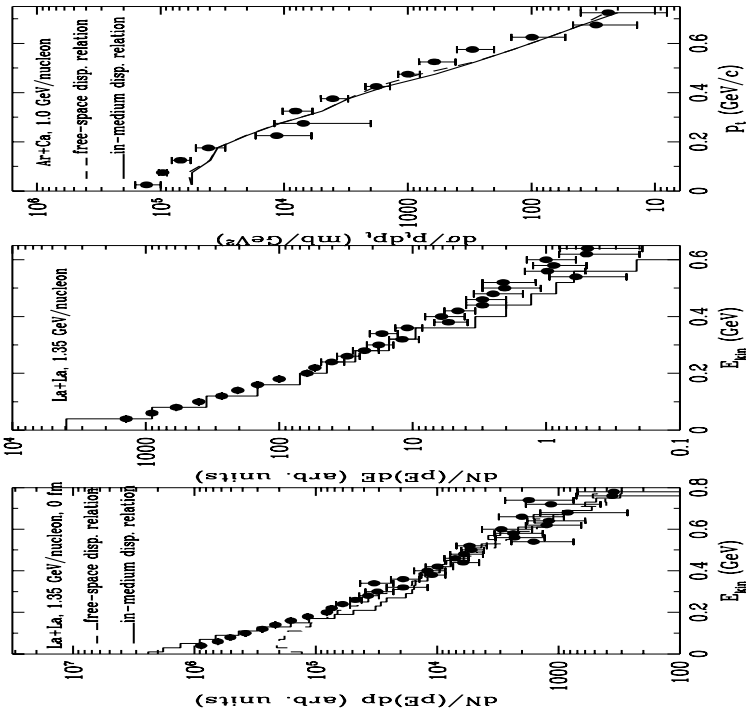

Fig. 12 Pion transverse kinetic energy spectra in La+La collisions at 1.35 GeV/nucleon and in Ar+Ca collisions at 1 GeV/nucleon. The left, middle, and right panels are from Refs. [53], [220], and [280], respectively. The experimental data from Ref. [54] for La+La collisions and from Ref. [55] for Ar+Ca collisions are shown by solid circles.

It should be mentioned that there are still some controversies regarding transport model calculations of pion spectra in heavy-ion collisions. For example, in Ref. [220] enhanced soft pions can also be obtained by treating pions as free particles. This is shown in the middle panel of Fig. 12 for La+La collisions at 1.35 GeV. The low-momentum pions were found to come mainly from the decay of delta resonances at freeze-out. However, this was not confirmed in similar transport model calculations by other groups [53,280,283].

Furthermore, the effects of a modified pion dispersion relation in medium on pion spectra do not all agree. In Ref. [280], this effect is found to be very small due to a different treatment of the in-medium pion dispersion relation in the transport model. This is shown in the right panel of Fig. 12 where the solid and dashed curves are theoretical results obtained with the in-medium and the free-space pion dispersion relation, respectively. Therefore, further work on quasipions in transport models are required, and this has recently been taken up in Ref. [285].

Medium effects on pion (also kaon) momentum spectra in hot hadronic matter have been investigated in Refs. [281,282] based on the 'optical potential' constructed from the forward scattering amplitude. The attractive pion collective potential was proposed in Ref. [281] as a possible explanation for the observed enhancement of low transverse momentum pions (the soft pion puzzle) in heavy-ion collisions at SPS energies [273], in much the same way the attractive pion potential leads to enhanced soft pions in heavy-ion collisions at SIS energies. However, it was shown in Ref. [286] that in order for this attractive potential to be effective in cooling down pions, the colliding system has to expand slower than the speed of these low-momentum pions. Since at SPS energies, the system and hence the source

of the pion potential is made of pions as well, it is unlikely that the above condition can be satisfied.

5. collective flows

Besides particle spectra, the collective motion of particles and fragments, both in and out-of the reaction plane, has been extensively studied in heavy-ion collisions at SIS energies [56,57,201,202,287–294]. It has been shown that the proton (and fragment) flow is sensitive to both the density (related to the nuclear equation of state) and momentum dependence of the nuclear potential [201], as well as the in-medium NN cross sections [295–297]. Pion flow has also been identified in heavy-ion collisions, and is seen to undergo a transition from flow at small impact parameters to antiflow at large impact parameters as a result of the shadowing effects from the spectator nucleons [283,292,293]. Antiproton and antikaon flows in heavy-ion collisions have been seen in both the RQMD [294] and the relativistic hadronic cascade (ARC) [216] calculations. Because of their large annihilation cross section, both antiproton and antikaon flows are found to be opposite to that of nucleons. Kaon flow has recently been proposed as another observable for studying the kaon properties in dense matter [56], and is being studied experimentally by both the FOPI [57] and the EOS [289] collaboration in heavy-ion collisions at a few GeV/nucleon.

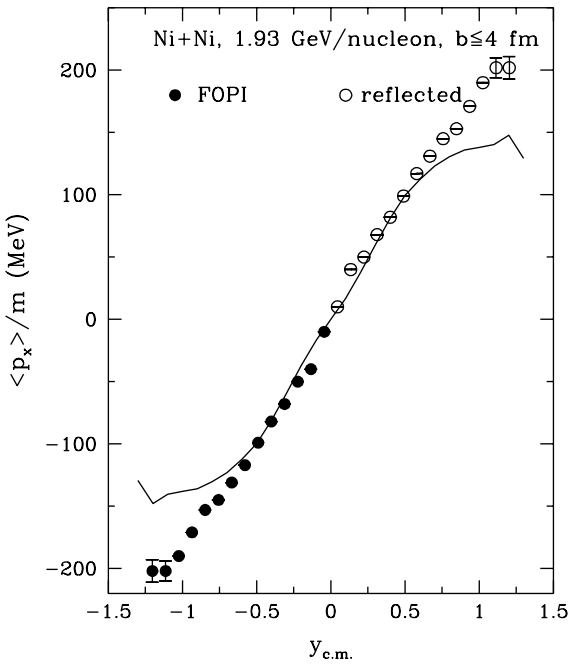

Fig. 13 Proton average in-plane transverse momentum from Ni+Ni collisions at 1.93 GeV/nucleon. The experimental data from the FOPI collaboration [57] are shown by circles.

In-plane particle flow is usually shown as the average in-plane transverse momentum $\langle p_x \rangle$ as a function of rapidity y. The results for proton flow in Ni+Ni collisions at 1.93 GeV/nucleon using the relativistic transport model with

a soft EOS are shown in Fig. 13. They are obtained after taking the impact-parameter-weighted average over b$\leq$ 4 fm, corresponding approximately to the centrality selection in experiments by the FOPI collaboration [57]. Both the experimental data, shown in the figure by solid circles, and the theoretical results include a low transverse momentum cut of $p_t > 0.5m_N$. It is seen that the theoretical predictions are in good agreement with the data except at the projectile and target rapidities where there are some differences, which are not understood at present.

To extract nuclear equation of state at high densities, proton flow has also been studied extensively in nonrelativistic transport models with the inclusion of a momentum-dependence in the nuclear potential [201,202]. The results of Refs. [201] and [202] are shown in the left and right panels of Fig. 14, respectively. The flow parameter F in these work is defined by the average transverse velocity $\langle p_x \rangle/m$ at $y = 0$. The momentum-dependence in the nuclear mean field was found to be important in reproducing correctly the dependence of the flow parameter on the incident energy and the colliding system. It is seen that the soft EOS with a compression modulus of about 200 MeV gives a good fit to the experimental data from both Nb+Nb and Au+Au collisions.

In Fig. 15, pion flow in Au+Au collisions at 1 GeV/nucleon and impact parameters b =3, 6, 9 fm is shown. In central collisions (dotted curve), pions are seen to follow the flow of nucleons, while in mid-central (dashed curve) and peripheral (solid curve) collisions, the pion flow direction is opposite to that of nucleons. This transition from flow in central collisions to antiflow in mid-central and peripheral collisions has also been predicted in Refs. [283,293]. The 'anticorrelation' of pions to nucleons at large impact parameters is mainly due to the rescattering and absorption of pions by the spectator nucleons.

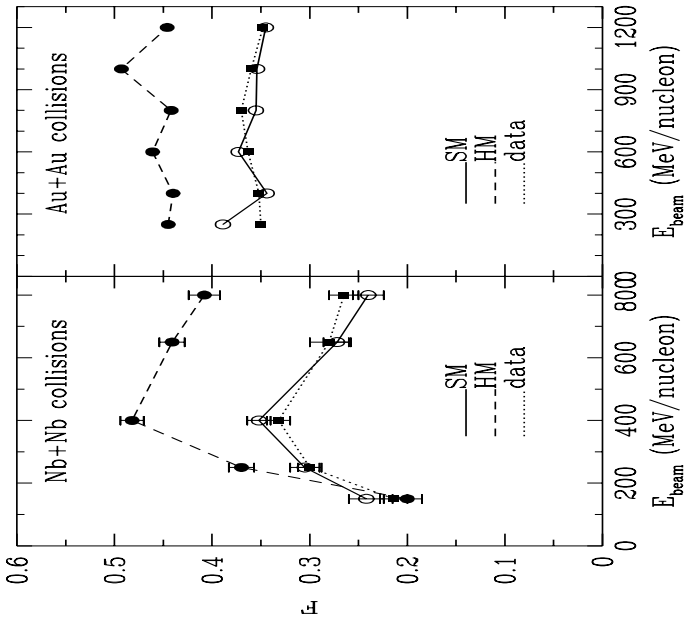

Fig. 14 Proton flow parameter F as a function of the incident energy for Nb+Nb (from Ref. [201]) and Au+Au collisions (from Ref. [202])

Fig. 16 shows the average transverse momentum of kaons in the reaction plane as a function of the center-of-mass rapidity y_{cm} in Ni+Ni collisions at 1.93 GeV/nucleon and for impact parameters b$\leq$4 fm. The dotted curve, corresponding to the case without kaon potential, shows that kaons flow in the same direction as nucleons but with a smaller flow velocity. The results with only the kaon vector potential are shown by the dashed curve. The kaon flow in this case is opposite to that of nucleons, i.e., the appearance of an 'antiflow' of kaons with respect to nucleons. With a weak repulsion due to both scalar and vector potentials, it is seen that the kaon flow, shown by the solid curve, is in the same direction as that of nucleons but its strength is significantly reduced. Thus, the repulsive kaon potential tends to make kaons flow away from nucleons, and its effect depends sensitively on the strength of the kaon potential. It is therefore possible to study the kaon potential in nuclear medium by measuring kaon flow in heavy-ion collisions. Preliminary data from the FOPI collaboration [57], shown by the solid circles with error bars, seem to be consistent with the existence of both scalar and vector potentials for a kaon in nuclear medium.

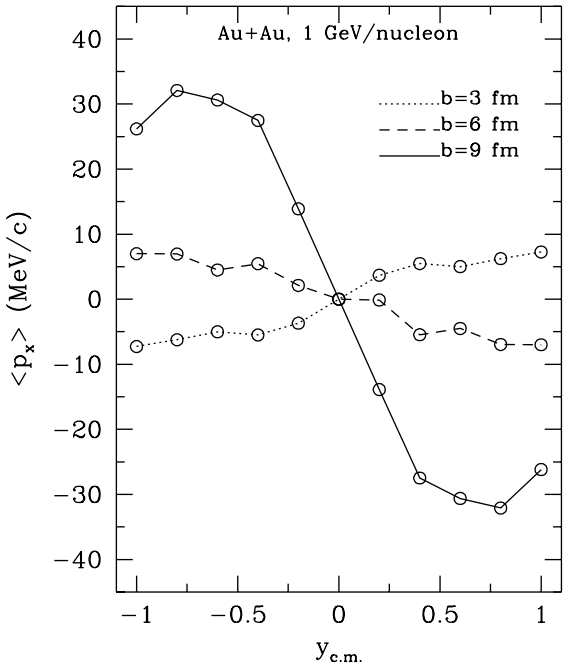

Fig. 15 Pion average in-plane transverse momentum as a function of rapidity from Au+Au collisions at 1 GeV/nucleon and impact parameters b=3 (dotted), 6 (dashed), and 9 (solid) fm. (from Ref. [56])

With the confirmation of potential effects on kaon flow in heavy-ion collisions, it is interesting to note that the attractive antikaon and antiproton potentials in nuclear medium are expected to change the antiflow of these particles caused by their shadowing from nucleons as a result of large absorption cross sections. Indeed, it has been recently shown that including the attractive potential given by the chiral Lagrangian, the strong antikaon antiflow is seen to change into a weak flow [298]. Similar medium effects have been shown for pion flow in the QMD calculations with an in-medium pion dispersion relation [299].

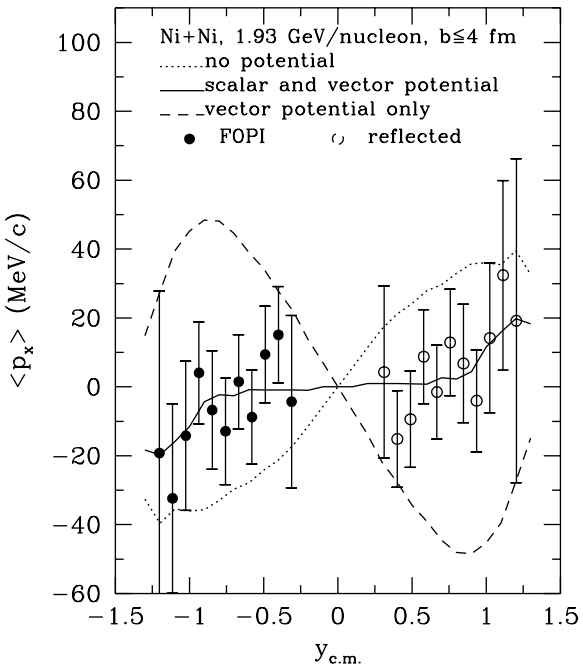

Fig. 16 Kaon average in-plane transverse momentum as a function of rapidity from Ni+Ni collisions at 1.93 GeV/nucleon. The experimental data from the FOPI collaboration [57] are shown by circles.

B. heavy-ion collisions at AGS and SPS energies

Ultra-relativistic heavy-ion collisions have been carried out at AGS with a beam energy of about 10 GeV/nucleon and at SPS with an incident energy of about 200 GeV/nucleon. The main motivation for carrying out these experiments at increasingly higher energies is to create and study in the laboratory the quark-gluon plasma, which is believed to exist in the early evolution of the universe at about one micro second after the Big Bang. At these energies, the reaction dynamics becomes much more complex than that at SIS energies, as many hadrons, such as eta, kaon, antikaon, rho and omega as well as other higher baryon resonances, are abundantly produced, and we thus need to include them explicitly. Since the interactions among these hadrons are not well understood, various assumptions have been introduced to relate the unknown ones to the known ones. Nevertheless, cascade-type models have been developed and seem to describe the global features of heavy-ion collisions at both AGS and SPS energies reasonably well [97,181,182]. In this subsection, we shall discuss some selected topics such as the strangeness enhancement, the difference in the slope parameters of K^+ and K^- momentum spectra, and the enhancement of very low momentum kaons.

1. Kaon enhancement

In heavy-ion collisions at AGS energies, the K^+/π^+ ratio has been found to be enhanced relative to that from proton-nucleus collisions [63,64]. Different mechanisms have been proposed to explain this enhancement. In RQMD [182,300], it is attributed to meson-baryon interactions in the collision. In ARC [181], it is due to interactions between baryon resonances created in the early stage of the collision. In a most recent relativistic transport model (ART) [97], significant contributions are found not only from the baryon-baryon and meson-baryon interactions but also from the meson-meson interaction. On the other hand, it has been shown in Ref. [301] that the measured kaon yield can be explained by a simple fireball model at both thermal and chemical equilibrium. Since all models predict a more or less equilibrated system at freeze out, it is thus difficult to verify from the kaon yield which models correctly describe the kaon production mechanism. Furthermore, in these models the energy density reached in the early stage of the collision when most kaons are produced have been found to exceed the one believed to be for a quark-gluon matter. The conclusions drawn from these models are thus expected to change when a more proper treatment of the initial stage is included.

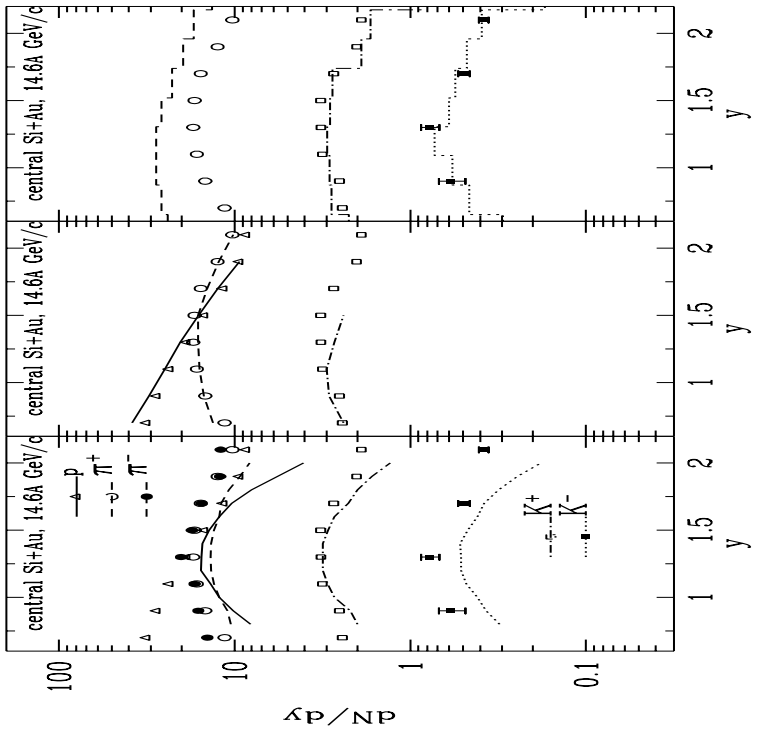

Fig. 17 Particle rapidity distributions in central Si+Au collision at 14.6 GeV/c/nucleon. The left, middle, and right panels are from Refs. [61], [181], and [300], respectively. The experimental data from Ref. [64] are also shown.

To understand the enhanced kaon production, the relativistic transport model has been used to study the expansion stage of heavy-ion collisions at these energies by assuming that a fireball is formed in the initial stage [60,61]. The fireball then expands, and kaons and antikaons are produced from baryon-baryon, meson-baryon, and meson-meson interactions. Both kaons and antikaons with in-medium masses propagate through the hadronic matter under the

influence of the mean-field potentials and undergo collisions with both nucleons and pions. Furthermore, antikaons can be destroyed via the reaction $\bar{K}N \to \pi Y$.

In the left panel of Fig. 17, the particle rapidity distributions from Ref. [61] are compared with the experimental data from Ref. [64]. One sees that good agreements with the experimental data are obtained for pions, kaons, and antikaons. The failure of the calculated proton distribution at smaller rapidities is due to the neglect of protons from the target spectator in the fireball approach. In this model study, a significant number of kaons are produced from meson-meson interactions which become important as a result of reduced total kaon-antikaon masses in dense matter [136].

In the middle panel of Fig. 17, the results from the ARC model of Ref. [181] are compared with the experimental data for proton, π^+ and K^+. Medium effects are neglected in this cascade-type calculation. Kaons are found to be mainly (about 70%) produced from the interactions between baryon resonances. The results from the RQMD calculation [300] for π^+, K^+, and K^- are shown in the right panel of Fig. 17. Again, the enhanced kaon production can be well described. In the RQMD, kaon production from baryon-meson collisions is found to be important. Similar results have been obtained in the ART calculation of Ref. [97]. The successful description of the kaon data by cascade-type calculations, however, does not rule out the mechanism proposed in Ref. [60]. If the mass of $K\bar{K}$ decreases as a result of chiral symmetry restoration, more kaons are produced, but they will be destroyed by reverse processes to maintain chemical equilibrium. One thus needs to look at other observables, such as the phi meson yield as it is sensitive to the change of $K\bar{K}$ energy as a result of the small difference, about 30 MeV, between the phi meson mass and the sum of K and $\bar{K}$ masses. The dilepton spectra from kaon-antikaon annihilation will also be useful, as it shows directly the invariant mass of the kaon-antikaon pair through the phi meson peak.

2. Difference in the slope parameters of kaon and antikaon transverse mass spectra

In Ref. [61], the transverse mass spectra of particles have also been calculated in the fireball model, and they are shown in Fig. 18. All particles have essentially exponential distributions. The slope parameters for kaons and antikaons show the difference expected from mean-field effects, i.e. the effective temperature of antikaons is lower than that of kaons. This can be understood as follows: Consider antikaons with high initial energies in the fireball that is formed in the collision. They move relatively fast and escape thus from the fireball while its size has increased only slightly. But these antikaons must use up much of their kinetic energies to climb out of the deep potential well so that the measured kinetic energies are substantially smaller. On the other hand, low energy antikaons stay in the fireball and escape later in time when the fireball size is large and the mean-field potential becomes negligible small. These antikaons therefore do not loose much energy. The net effect is that the apparent temperature of antikaons after freeze out is lower than the initial temperature. For kaons, the potential is only slightly repulsive because of cancellation between the attractive scalar field and the repulsive vector field. The change of kaon apparent temperature is thus very small. If antikaons and kaons have similar initial temperatures, then one expects to see a lower final temperature for antikaons than for kaons.

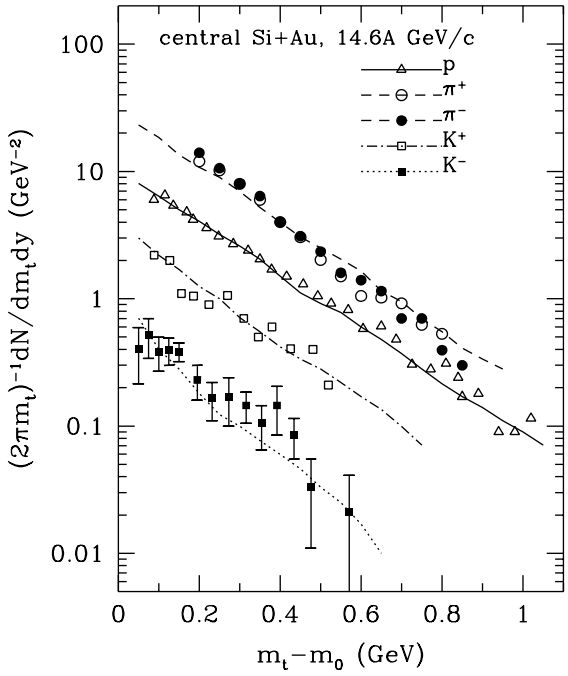

Fig. 18 Particle transverse energy spectra from central Si+Au collisions. (from Ref. [61])

Similar effects are seen for antiprotons. The deep attractive mean-field potential for antiprotons makes their apparent temperature much lower than that for protons [62]. All these results seem to be supported by the experimental observations.

We note that the above discussions are for Si+Au collisions. For Au+Au collisions at AGS energies, the initial compression is expected to be much more appreciable than in Si+Au collisions, so a larger radial expansion may appear and thus reduces the effects of mean-field potential on particle spectra [286].

3. cool kaons

Another interesting preliminary experimental observation in heavy-ion collisions at AGS energies is the enhancement of low transverse mass (m_t) K^+ and K^- in Si+Pb collisions at 14.6 (GeV/c)/nucleon by the E814 collaboration [302]. The spectra of these extremely cold kaons can be characterized by an inverse slope parameter (temperature) as low as 15 MeV, which is about one order-of-magnitude smaller than the temperature of normal kaons measured in earlier AGS experiments [63]. These low m_t kaons cannot be obtained in conventional models such as RQMD [182], ARC [181], and ART [97]. Although this experimental result has not been unambiguously confirmed by other experiments [303], it has already generated some interesting theoretical explanations.

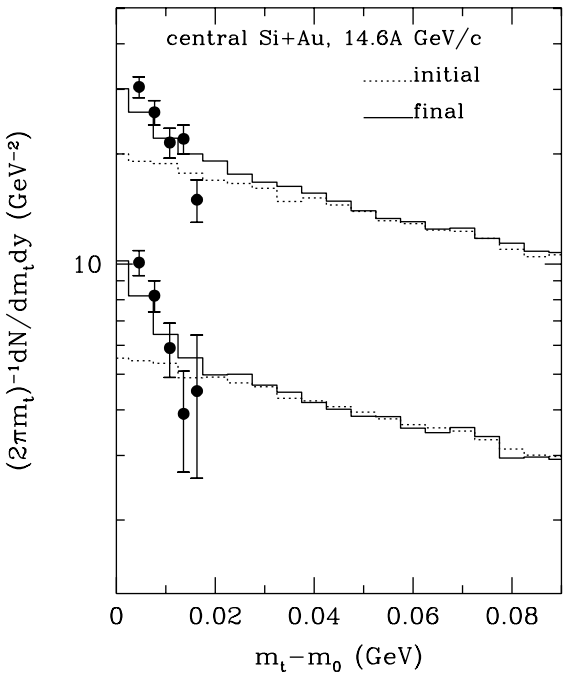

Fig. 19 Initial (dotted) and final (solid) kaon and antikaon transverse energy spectra. The experimental data are from [302]. (from Ref. [307])

Based on the Georgi vector limit of the hidden gauge theory, Brown and Rho [304] have argued that the vector interaction vanishes when the chiral symmetry is restored. This seems to be supported by calculations based on effective hadronic models for the vector coupling constant in medium [305]. If this is indeed the case, then one expects that the kaon potential will become attractive at very high density and temperature as the scalar attraction becomes dominant. This idea was first adopted by Koch [306], who considered the temperature effects, to explain the appearance of these low energy kaons. In Ref. [307], the density effect is emphasized. Because of the reduced vector potential, the nuclear equation of state becomes softened, leading to the possible formation of a density isomer. As a result, the initial expansion of the nuclear matter is relatively slow so that kaons and antikaons can be effectively cooled by the attractive mean-field potentials. This effect has been studied in the relativistic transport model [307] by assuming that the system is initially in the density isomer. The results are shown in Fig. 19 and compared with the preliminary E814 data. For both kaons and antikaons, one obtains in the final transverse mass spectra a cold low-m_t component as observed in the experiment.

4. strangeness enhancement in heavy-ion collisions at SPS energies

In heavy-ion collisions at SPS energies, enhanced production of strange particles have also been observed. For example, the antilambda yield in the NA35 experiment of S+S at 200 GeV/nucleon [73] is 1.5 per event and is 115 times greater than that in p-p collisions at same energy. Compared with the 36-fold enhancement of negatively

charged particles, most of them being negative pions, there is a factor of three enhancement of antilambda yield in these collisions. This enhancement can be explained if one simply assumes that a quark-gluon plasma is formed in the initial stage of the collisions. Other explanations have also been proposed. Aichelin and Werner have emphasized the importance of many-body cluster effects [308]. Sorge *et al.* [309] have shown that the formation of a color rope from string excitations can lead to enhanced production of antilambdas. In Ref. [72], this enhancement is explained by the lower antilambda production threshold as a result of reduced antilambda mass in dense matter. In a simplified hydrochemical model, the process $KM \to \bar{\Lambda}N$, where M denotes either a pion or a rho meson, gives an enhanced antilambda production in the collision. A similar explanation based on the relativistic mean field theory has been proposed in Ref. [310].

The reduced phi meson mass in medium has also been shown to lead to an enhanced phi meson production in CERN heavy-ion collisions [70,71].

C. dilepton production in heavy-ion collisions

Since dileptons are not subject to the strong final-state interactions associated with hadronic observables, they are the most promising probe of the properties of hot dense matter formed in the initial stage of high energy heavy-ion collisions. Dileptons have thus been proposed as useful observables for studying medium modifications of the pion dispersion relation at both finite density and temperature [311,312], the in-medium properties of vector mesons [58,313–316], and the phase transition from the hadronic matter to the quark-gluon plasma [317–321].

There are many sources for dilepton production in hadronic matter. These include the proton-neutron and pion-nucleon bremsstrahlung, the Dalitz decay of pions, etas, and deltas, the direct decay of vector mesons, as well as the pion-pion and kaon-antikaon annihilation that proceed through the formation of vector mesons. To study the in-medium properties of vector meson properties, the pion-pion and kaon-antikaon annihilation are most important due to vector dominance in the pion and kaon electromagnetic form factors. Neglecting lepton masses, the dilepton production cross section from the annihilation of two pseudoscalar meson P through a vector meson V is given by

$$\sigma_{PP\to V\to l^+l^-} = a\frac{8\pi\alpha^2 k}{3M^3}\frac{m_V^4}{(M^2-m_V^2)^2+(m_V\Gamma_V)^2}. \tag{65}$$

In the above, M is the invariant mass of the lepton pair, α is the fine structure constant, and k is the three-momentum of the pseudoscalar meson in the center-of-mass of the vector meson. The mass and width of the vector meson are denoted by m_V and Γ_V, respectively. The value of a is 1 and 1/9 for $\pi^+\pi^- \to \rho^0 \to e^+e^-$ and $K^+K^- \to \phi \to e^+e^-$ ($K^0\bar{K^0} \to \phi \to e^+e^-$), respectively. In this "form factor" approach, the formation time of the dilepton is neglected and the effect of the intermediate vector meson is included through the electromagnetic form factor. This is a reasonable approach for the case without medium effects.

With medium-dependent vector meson masses, one needs to adopt the "dynamical approach" by including explicitly the formation, propagation and decay of the intermediate vector meson so that the change of its properties in medium can be included. In this approach, the vector meson formation cross section from the meson-meson annihilation is given by

$$\sigma_{PP\to V} = b\frac{6\pi}{k^2}\frac{(M\Gamma_V)^2}{(M^2-m_V^2)^2+(m_V\Gamma_V)^2}, \tag{66}$$

where b is 2 and 1 for $\pi^+\pi^- \to \rho^0$ and $K^+K^- \to \phi$ ($K^0\bar{K}^0 \to \phi$), respectively. The decay width of a vector meson of mass M to the dilepton is given by [142]

$$\Gamma_{V\to l^+l^-} = a\frac{4\pi\alpha^2}{g_{VPP}^2}\frac{m_V^4}{3M^3}, \tag{67}$$

where the coupling constants are $g_{\rho\pi\pi}/4\pi \approx 2.9$ and $g_{\phi KK}/4\pi \approx 1.7$, determined by their respective decay widths.

We note that in the dynamical approach the vector meson mass and width in Eqs. (66) and (67) are evaluated using the local density at the time of its formation and decay, which may be different due to the change in density. It has been found in Ref. [58] that for vector mesons with large decay widths (e.g., the rho meson), the form factor approach gives results qualitatively similar to the dynamical approach. However, for mesons with small decay widths (e.g., the phi meson), the dynamic approach is required as the medium effects are overestimated in the from factor approach.

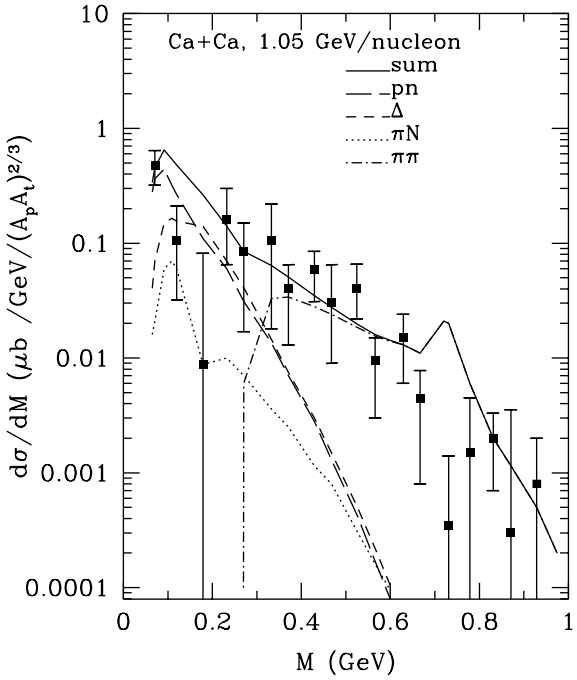

Fig. 20 Dilepton invariant mass spectrum from Ca+Ca collisions at 1.05 GeV/nucleon. The experimental data from the DLS collaboration [322] are given by solid squares while the theoretical total yield is given by the thick solid curve. (from Ref. [218])

In the following, dilepton production from heavy-ion collisions at SIS/GSI, SPS/CERN, and RHIC/BNL is studied in the relativistic transport model, and the results are compared with available experimental data.

Dileptons have been measured from heavy-ion collisions at Bevalac by the DLS collaboration [322]. The experimental dilepton invariant mass spectrum from Ca+Ca collisions at 1.05 GeV/nucleon is shown in Fig. 20. Based on transport models, perturbative calculations of dilepton production, including contributions from proton-neutron bremsstrahlung, pion-nucleon interactions, delta and eta decays, and pion-pion annihilation, have been carried out in Refs. [218,323,324]. A typical result from Ref. [218] is shown in Fig. 20. It is seen that dileptons with small invariant masses are mainly from proton-neutron bremsstrahlung and delta decays while dileptons with large invariant masses are dominated by pion-pion annihilation. The contribution from eta decays, that was neglected in Ref. [218], turns out to be very important for invariant masses below about 500 MeV [324]. Nevertheless, the eta has a width of only 1.2 keV and decays thus outside of the matter. Its contribution to dilepton production can in principle be subtracted out if its spectrum is also measured. We also see clearly the rho meson contribution to dilepton production from pion-pion annihilation as a result of rho meson dominance in the pion electromagnetic from factor. The data are, however, not accurate enough to extract the in-medium rho meson properties.

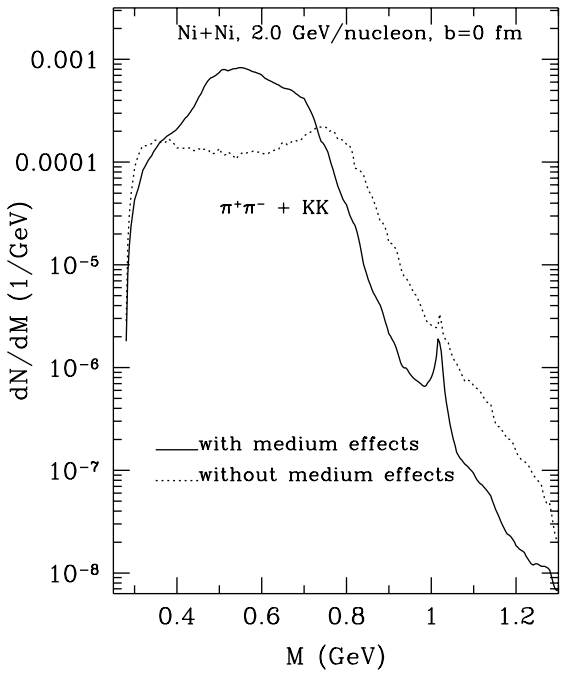

Fig. 21 Dilepton invariant mass spectra from pion-pion and kaon-antikaon annihilation in Ni+Ni collision at 2 GeV/nucleon and impact parameter b=0 fm. The dashed and solid curves are obtained using free and in-medium meson masses, respectively. (from Ref. [58])

Future experiments at SIS with the HADES detector [59] will provide data with vastly improved statistics to allow us to study more clearly the medium effects on vector meson properties. To see the medium effects in these experiments, the dilepton invariant mass spectra from Ni+Ni collisions at an incident energy of 2 GeV/nucleon and

impact parameter of 0 fm with free vector meson masses (dashed curve) and in-medium vector meson masses given by Eqs. (43) and (44) from the QCD sum rules (solid curve) have been calculated [58] and are shown in Fig. 21. For pion-pion annihilation, medium effects shift the rho meson peak to around 550 MeV, and its height increases by about a factor of four. For kaon-antikaon annihilation, the phi peak shifts slightly to a lower invariant mass, and its width is also broadened when medium effects are included. In addition, there appears a shoulder around 950 MeV. For a complete picture of dilepton production at SIS energies, contributions from other channels, such as the Dalitz decay, bremsstrahlung, vector mesons produced in initial nucleon-nucleon collisions, and vector mesons from decay of high resonances [325], need to be included.

For heavy-ion collisions at AGS energies, a similar shift of the rho meson strength to lower dilepton invariant masses has been seen in RQMD calculations using also the QCD sum-rule results for in-medium vector meson masses [326]. Since a omega meson has a much longer lifetime and decays mostly at freeze-out, an interesting phenomenon of ρ-ω splitting was seen in the dilepton spectra. It would be very useful if dilepton production from heavy-ion collisions at AGS energies could be measured.

2. dileptons from SPS/CERN

For heavy-ion collisions at SPS energies, hot and dense matter is also formed in the initial stage of the collisions. One expects that medium effects will lead to a shift of the vector meson peaks in dilepton invariant mass spectra. Experiments from both the CERES [67] and the HELIOS-3 [68] collaboration have shown that there is an excess of dileptons over those known and expected sources which cannot be explained by uncertainties and errors of the normalization procedures [69]. In particular, in the CERES experiment for central S+Au collisions at 200 GeV/nucleon, a significant enhancement of dileptons with invariant masses between 250 MeV to 1 GeV over that from the proton-nucleus collision has been found.

These experimental data have generated a great deal of interest in the heavy-ion community. Different models, ranging from schematic estimates based on a possible enhancement of η and η' production [327,328], to hydrodynamical models [329,330], and relativistic transport models [65,66,331–333], have been used to study this phenomenon. Although the contribution from pion-pion annihilation, that has not been included in the 'cocktail' of the CERES collaboration, was found to be important for low-mass dileptons, the data in the low mass region are still above the theoretical results from these calculations when vector meson properties in free space are used. This situation is summarized in ig. 22 where the results from Ref. [66] (solid curve) using the relativistic transport model with initial conditions determined by the RQMD, Ref. [331] (dashed curve) from the Hadron-String Dynamics, and Ref. [329] (dotted curve) from the hydrodynamical model are shown together with the CERES data. It is seen that in all three studies the calculated low mass dileptons are by about a factor of 2-4 below the data, and for dileptons around $m_{\rho,\omega}$ they are slightly above the data. It is also of interest to note that the three calculations, although with different dynamical models, agree more or less with each other, and the differences are less than 20%. A strong peak around m_ϕ in the results of Ref. [329] will become a bump once the mass resolution of the CERES collaboration is properly included.

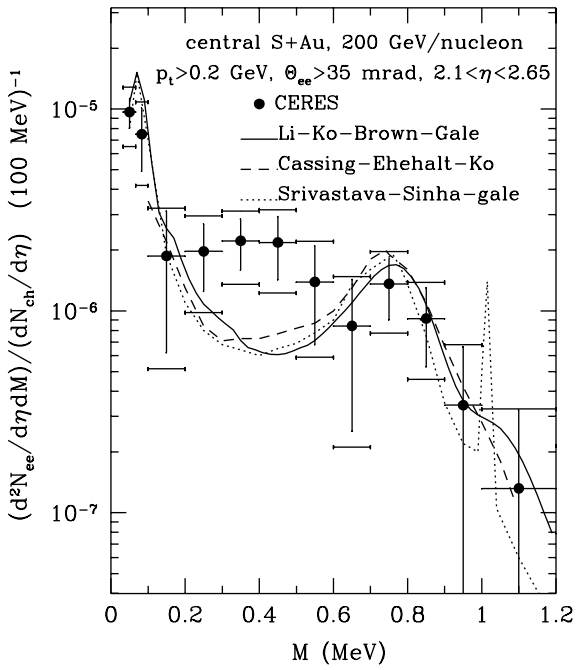

Fig. 22 Dilepton invariant mass spectra in central S+Au collisions at 200 GeV/nucleon with free meson masses. The solid, dashed, and dotted curves are from Refs. [66], [331], and [329], respectively. The experimental data from the CERES collaboration [67] are shown by solid circles, with bars denoting the statistical errors while the systematic uncertainties are given by brackets.

The results using in-medium vector meson masses are shown in Fig. 23 by the solid curve. The agreement with the experimental data is greatly improved. The enhancement at low invariant masses is due to both the shift of primary rho mesons to lower masses and pion-pion annihilation occurring in hot dense matter. Since pions have a thermal distribution, most pion pairs are of low invariant mass. When the rho-meson mass is reduced, its formation probability from pion-pion annihilation is enhanced, thus increasing the production of low-mass dileptons. The remaining peak around $m_{\rho,\omega}$ then comes from the decay of omega mesons which have a very small decay width, and therefore mostly decay at freeze out when their mass has returned to the free value. One notes that dileptons with invariant masses below about 300 MeV are mainly from the Dalitz decay of π^0, ω, and η.

Dimuon invariant mass spectra have been measured by the HELIOS-3 collaboration in S+W collisions at 200 GeV/nucleon [68]. The data also show an enhancement of dileptons around $M \approx 0.4 - 0.6$ GeV. This provides another possible indication that the vector (rho) meson mass might be reduced in hot dense medium. The comparison of theoretical results obtained from the relativistic transport model with the HELIOS-3 data is shown in Fig. 24 [66]. With free vector meson masses, the theoretical results are below the HELIOS data in the mass region from 0.35 to 0.6 GeV by about a factor of two, and slightly above the data around $m_{\rho,\omega}$. Using in-medium vector masses, we again see an enhanced dilepton production in the low mass region and a reduction around $m_{\rho,\omega}$. This brings the theoretical results in better agreement with the data. Similar results have been obtained in Ref. [332] using the Hadron-String

Dynamics.

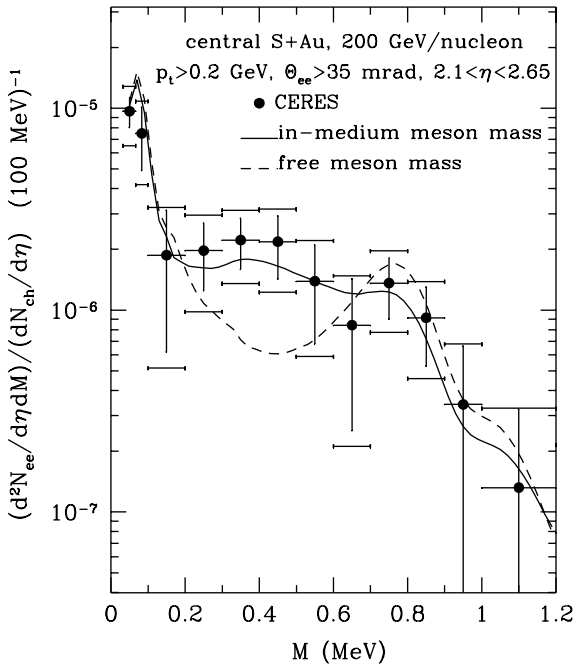

Fig. 23 Same as Fig. 22. The dotted and solid curves are obtained using free and in-medium meson masses, respectively. (from Ref. [66])

The medium effects seen in the HELIOS-3 case are smaller than that in the CERES case. This is due to the fact that in the HELIOS-3 experiment dileptons are measured at forward rapidity ($3.7 < \eta < 5.5$) where the charged-particle multiplicity is low, while in the CERES experiment they are measured in the midrapidity ($2.1 < \eta < 2.65$) with a higher charged-particle multiplicity. It is also of interest to note that the theoretical results from both Ref. [66] and Ref. [332] are well below the HELIOS-3 data above 1.2 GeV. This may indicate the importance of processes such as $\pi a_1 \rightarrow l^+l^-$ [334,335] and the decay of heavier vector mesons such as $\omega(1390)$ [336,337]. Also, in this mass region, the contribution from the quark-gluon plasma and the initial Drell-Yan processes might become important.

3. dileptons from RHIC/BNL

In heavy-ion collisions at the Relativistic Heavy-Ion Collider (RHIC) being constructed at the Brookhaven National Laboratory, dileptons will be measured as they are likely to carry the signature for the quark-gluon plasma expected to be created in the collisions [317–319,321]. However, there are a number of different sources of dileptons in heavy-ion collisions at these energies. For dileptons with low invariant mass, i.e., below about 1 GeV, they are dominated by hadronic processes, such as π^0 and η Dalitz decays as well as vector meson (ρ, ω, and ϕ) direct decays. For intermediate-mass dileptons, i.e., between 1 and 2 GeV, dilepton production from heavy meson resonances [335,336] and charmed meson (D and D^*) decays become important. It is in this invariant mass regions that it may be possible

to see dileptons emitted from the quark-gluon plasma via quark-antiquark annihilation if its temperature is sufficient high [338]. Above 2 GeV, dileptons are from Drell-Yan process involving the annihilation of quarks and antiquarks in the initial colliding nuclei. In this region of dilepton invariant mass, an interesting proposal to see the signature of the quark-gluon plasma is the J/Ψ suppression [339] due to its dissociation in the quark-gluon plasma as a result of color screening. Current experiments at CERN/SPS have indeed shown that the number of J/Ψ observed versus the Drell-Yan background is reduced by about a factor of 2 in heavy-ion collisions than in proton-nucleus reactions [340]. Unfortunately, the data can also be explained by hadronic absorption models [341–343].

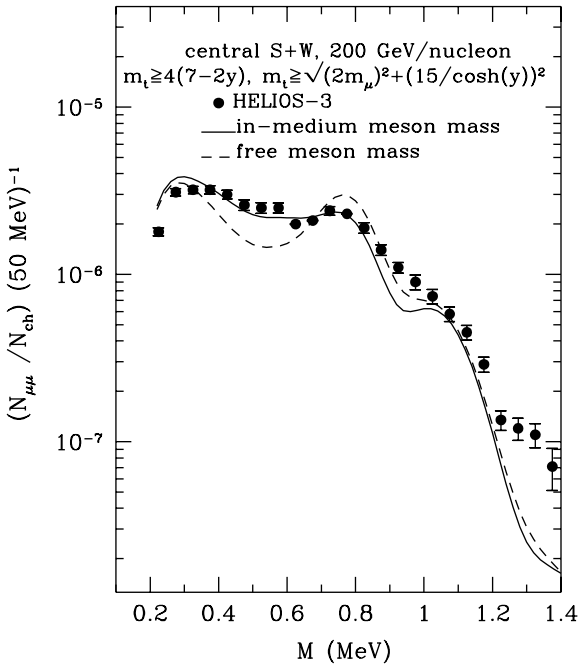

Fig. 24 Dimuon invariant-mass spectrum from pion-pion annihilation in central S+W collisions at 200 GeV/nucleon. The dotted and solid curves are obtained with free and in-medium masses, respectively. The experimental data from the HELIOS-3 collaboration [68] are shown by solid circles. (from Ref. [66])

On the other hand, the change of phi meson mass in hot matter as discussed in Sect. II.C has led to a new signature for identifying the quark-gluon plasma to hadronic matter phase transition in ultrarelativistic heavy-ion collisions [344]. In a boost invariant hydrodynamical calculation with transverse flow and including temperature-dependent vector meson masses, it has been found that a low mass phi peak at $\sim$ 880 MeV besides the normal one at 1,020 MeV appears in the dilepton spectrum if a first-order phase transition or a slow cross-over between the quark-gluon plasma and the hadronic matter occurs in the collisions. Assuming an initial temperature $T_i = 250$ MeV, a critical temperature $T_c = 180$ MeV, and a freeze out temperature $T_f = 120$ MeV, the results are shown by the solid curve in Fig. 25. The three peaks correspond to the omega, the low-mass phi, and the normal phi meson, respectively. Because of their reduced mass at finite temperature according to the QCD sum-rule studies [345], decays from rho

mesons lead to a broad distribution of dileptons at low masses.

The low-mass phi peak is due to the nonnegligible duration time for the system to stay near the transition temperature (about 10 fm/c) compared with the lifetime of a phi meson in the vacuum ($\sim$ 45 fm), so the contribution to dileptons from phi meson decays in the mixed phase becomes comparable to that from phi meson decays at freeze out. Also, its width from collisions with other hadrons remains small (about 10 MeV) [346,347].

Without the formation of the quark-gluon plasma, the low mass phi peak is reduced to a shoulder in the dilepton spectrum as shown by the dotted curve in Fig. 23, which is obtained by assuming that the initial temperature of the hadronic matter is just below T_c.

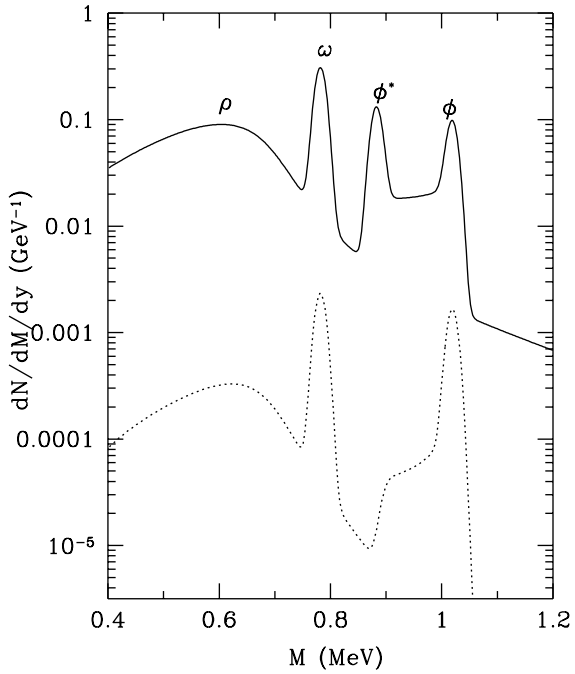

Fig. 25 Dilepton invariant mass spectra from ultrarelativistic heavy-ion collisions. Solid and dotted curves correspond to scenarios with and without the formation of a quark-gluon plasma, respectively. (from Ref. [344])

Since the transverse expansion velocity during the mixed phase is relatively small, the transverse momentum distribution of the low mass phi mesons is largely determined by the temperature of the mixed matter. The low mass phi mesons thus also provide information about the temperature at which the quark-gluon plasma to hadronic matter transition occurs.

V. SUMMARY AND OUTLOOK

Because of the partial restoration of chiral symmetry, the quark condensate decreases in hot dense matter. According to the prediction of QCD sum rules, hadron masses are then reduced in medium. As a result, the thresholds for particle production in medium are reduced, and the cross sections for their production are enhanced due to the increase of

phase space in the final states. The dense matter also gives rise to strong vector mean-field potentials. With these medium effects consistently included in the relativistic transport model, it has been shown that for heavy-ion collisions at SIS energies they can account for the observed enhancement of kaon, antikaon, and antiproton yields, the enhanced soft pions in the transverse direction, and particle flows in these collisions.

To place these conclusions on a firmer ground, a number of issues need to be addressed in future investigations. In heavy-ion collisions at SIS energies, the colliding system consists mainly of nucleons, baryon resonances, and pions. Particles can thus be produced from baryon-baryon, baryon-meson, and meson-meson collisions. Because of the small center-of-mass energy of the pion and the fact that pions materialize in the expansion stage of the collisions, hadron production from pion-pion interactions can be safely neglected at SIS energies. Kaon and antikaon production from pion-baryon collisions have been calculated and found to account for about 20% of their total yield. With improved experimental data, these contributions need to be more carefully studied. Similarly, antiproton production from pion-baryon collisions has not been considered and certainly need to be evaluated.

For subthreshold particle production, the most important contribution comes from baryon-baryon interactions, of which interactions involving baryon resonances are particularly important. One needs thus particle production cross sections in baryon-baryon collisions. For proton-proton collisions there exist empirical data for kaon, antikaon, and antiproton production, mostly at high beam energies [348]. The general strategy in the transport model is to introduce a parameterization for these data and then to extrapolate it to the threshold. The production cross section near the threshold then depends on the way the parameterization and extrapolation are introduced. This is particularly serious for antiprotons since there are essentially no experimental data below 20 GeV. Moreover, no experimental data exist for particle production from baryon-baryon collisions involving baryon resonances. Various assumptions have been made to relate these cross sections to that in proton-proton collisions. The validity of these assumptions certainly need to be carefully assessed. Also, the role of baryon resonances that are higher than the delta needs to be further investigated [349,350].

For antikaon and antiproton, there is an additional complication from their large annihilation cross sections. This raises the question of numerically how to accurately treat the annihilation process in transport models. Indeed, different treatment of antiproton annihilation could lead to almost an order of magnitude difference in the final antiproton survival probability [51,52,241,242,351]. Moreover, the antikaon and antiproton annihilation cross sections might be modified in medium due to changes in their masses, the screening effects from mesons [181], and the effect of Bose-Einstein enhancement in the final state [352]. For antiproton annihilation, which leads to about five pions, the latter effect is expected to be important in heavy-ion collisions at AGS and SPS energies as the abundance of pions is large in these collisions.

The medium modification of hadron masses has so far been included in transport models only in a minimum way by changing the threshold of particle production. In terms of Feynman diagrams, this amounts to change only the masses of the initial and final hadrons. In principle, the properties of exchanged particles can also be modified [60,231]. Besides changes of hadron masses, the coupling constants and the form factors in the vertices of Feynman diagrams might be modified in medium as well. All these need to be consistently studied.

Finally, off-shell propagation of particles has been neglected in all transport models. This effect on subthreshold particle production has been shown to be small [353]. However, off-shell effects due to correlations in the initial wave function may be important and need to be further studied.

For heavy-ion collisions at AGS energies, medium effects can also explain the enhanced K^+/π^+ ratio, the difference between the slope parameters of K^+ and K^- transverse kinetic energy spectra, the lower apparent temperature of antiprotons than that of protons, and the cool kaons with low transverse masses. However, these studies have been based on a fireball initial conditions so the initial nonequilibrium dynamics is not included. There are already models, such as the RQMD [182], ARC [181], and ART [97], which can treat the initial stage of heavy-ion collisions at these energies as enough inelasticity has been introduced in these models. It will be useful to extend the relativistic transport model by including these additional processes so both the collision dynamics and medium effects can be properly included.

Medium effects are also relevant for heavy-ion collisions at higher energies from the SPS at CERN. The reduced particle production thresholds in medium have been found to lead to enhanced production of phi mesons, antilambdas, and low-mass dileptons. As in the case of heavy-ion collisions at AGS energies, the relativistic transport model at its present form can only describe the expansion stage of these collisions. In the initial nonequilibrium stage, particle production from string fragmentation has shown to be essential [182]. It is thus again important to extend the relativistic transport model to include consistently in the initial stage the string dynamics. Such a step has already being taken by Cassing *et al.* [354].

We have shown in this review that high energy heavy-ion experiments offer the possibility to study the properties of hadrons in the hot dense matter formed in the initial stage of the collisions. This study is not only of interest in its own right but also important for future heavy-ion experiments at ultrarelativistic energies where the quark-gluon plasma is expected to be formed. To find the signatures of the quark-gluon plasma, it is essential to have a good understanding of the hadronic matter that exists both in the initial and final stages of heavy-ion collisions. Moreover, the modification of hadron properties in hot dense matter is expected to give rise to new signals for the quark-gluon to hadronic matter transition. For example, a low mass phi peak besides the normal one has been predicted to appear in the dilepton invariant mass spectra from ultrarelativistic heavy-ion collisions as a result of the decay of phi mesons with reduced in-medium mass during the transition. Furthermore, measurements of the transverse momentum distribution of these low mass phi mesons offer a viable means for determining the temperature of the transition.

However, experience from heavy-ion collisions at SIS, AGS, and CERN energies has shown that to extract useful physics from heavy-ion collisions requires transport models which can describe properly the entire collision dynamics. The same is expected for heavy-ion collisions at RHIC, so it is important to have a model which includes the initial parton cascade [355], the evolution of the resulting quark-gluon matter [356], the dynamics of hadronization [357], and the final hadronic dynamics. In this respect, the relativistic transport model developed extensively for low energy heavy-ion collisions provides a link of future developments in ultra-relativistic transport model to the experimental observations.

ACKNOWLEDGMENTS

We are grateful to J. Aichelin, M. Asakawa, G. E. Brown, W. Cassing, X. S. Fang, V. Koch, B. A. Li, R. Machleidt, U. Mosel, C. Song, H. Sorge, and L. Xiong for discussions and/or collaboration. We also thank our experimental colleagues, D. Best, P. Braun-Munzinger, A. Dress, E. Grosse, I. Kralik, M. Murray, J. Ritman, P. Senger, I. Tserruya,

T. Ullrich, K. Wolf, and P. Wurm for helpful discussions and/or communications. This work was supported in part by the National Science Foundation under Grant No. PHY-9509266. C.M.K. also acknowledges the support by the Alexander von Humboldt Foundation.

---

[1] J. F. Donoghue, E. Golowich, and B. R. Holstein, *Dynamics of standard model*, (Cambridge University Press, Cambridge, 1992).

[2] C. Bernard, M. C. Ogilvie, T. A. DeGrand, C. Detar, S. Gottlieb, A. Krasnitz, R. L. Sugar, and D. Toussaunt, Phys. Rev. D **45**, 3854 (1992).

[3] P. Gerber and H. Leutwyler, Nucl. Phys. **B321**, 387 (1989); J. Gasser and H. Leutwyler, Phys. Lett. **B184** (1989) 83.

[4] J. Wambach, in *Proc. of International Workshop XXIII on Gross Properties of Nuclei and Nuclear Excitations*, ed. H. Feldmeier and W. Nörenberg, p.21 (GSI, Darmstadt, 1995); G. Chanfry, M. Ericson, and J. Wambach, nucl-th/960704.

[5] E. G. Drukarev and E. M. Levin, Nucl. Phys. **A511**, 679 (1990).

[6] T. D. Cohen, R. J. Furnstahl, and K. Griegel, Phys. Rev. C **45**, 1881 (1992).

[7] M. C. Birse and J. A. McGovern, Phys. Lett. B **309**, 231 (1993).

[8] G. Chanfray and M. Ericson, Nucl. Phys. **A556**, 427 (1993).

[9] G. Q. Li and C. M. Ko, Phys. Lett. **B338**, 118 (1994).

[10] A. Delfino, J. Dey, M. Dey, and M. Malheiro, Phys. Lett. B **363**, 17 (1995).

[11] R. Brockmann and W. Weise, Phys. Lett. B **367**, 40 (1996).

[12] T. D. Cohen, R. J. Furnstahl, and D. K. Griegel, Phys. Rev. Lett. **67**, 961 (1991).

[13] T. Hatsuda and S. H. Lee, Phys. Rev. C **46** (1992) R34; T. Hatsuda, Nucl. Phys. **A544**, 27c (1992).

[14] W. Weise, Nucl. Phys. **A553**, 59c (1993).

[15] M. C. Birse, J. Phys. G **20**, 1537 (1994).

[16] G. E. Brown and M. Rho, Phys. Rep. **269**, 333 (1996).

[17] G. E. Brown, Nucl. Phys. **A522**, 397c (1991).

[18] C. M. Ko and G. Q. Li, in *Proc. of International Workshop on Multi-Particle Correlations and Nuclear Reactions,* ed. J. Aichelin and D. Ardouin, p. 215 (World Scientific, Singapore,1995).

[19] C. M. Ko and G. Q. Li, Nucl. Phys. **A583**, 591c (1995).

[20] H. Stöcker and W. Greiner, Phys. Rep. **137**, 277 (1986).

[21] G. F. Bertsch and S. Das Gupta, Phys. Rep. **160**, 189 (1988).

[22] W. Botermans and R. Malfliet, Phys. Rep. **198**, 115 (1990).

[23] W. Cassing, V. Metag, U. Mosel, and K. Niita, Phys. Rep. **188**, 363 (1990).

[24] J. Aichelin, Phys. Rep. **202**, 235 (1991).

[25] B. Blättel, V. Koch, and U. Mosel, Rep. Prog. Phys. **55**, 1 (1993).

[26] G. Peilert, H. Stöcker, and W. Greiner, Rep. Prog. Phys. **57**, 533 (1994).

[27] A. Bonasera, F. Gulminelli, and J. Molitoris, Phys. Rep. **243**, 1 (1994).

[28] C. M. Ko, Q. Li, and R. Wang, Phys. Rev. Lett. **59**, 1084 (1987); C. M. Ko, and Q. Li, Phys. Rev. C **37**, 2270 (1988); Q. Li, J. Q. Wu, and C. M. Ko, Phys. Rev. C **39**, 849 (1989); C. M. Ko, Nucl. Phys. **A495**, 321c (1989).

[29] H. Th. Elze, M. Gyulassy, D. Vasak, H. Heinz, H. Stöcker, and W. Greiner, Mod. Phys. Lett. **A2**, 451 (1987).

[30] B. Blättle, V. Koch, W. Cassing, and U. Mosel, Phys. Rev. C **38**, 1767 (1988).

[31] B. D. Serot and J. D. Walecka, Adv. Nucl. Phys. **16**, 1 (1986).

[32] B. D. Serot, Rep. Prog. Phys. **55**, 1855 (1992).

[33] G. Gelmini and B. Ritzi, Phys. Lett. **B357**, 431 (1995).

[34] G. E. Brown and M. Rho, Nucl. Phys **A596**, 503 (1996).

[35] R. J. Furnstahl, H. B. Tang, and B. D. Serot, Phys. Rev. C **52** 1368 (1995); Nucl. Phys. **A598**, 539 (1996).

[36] R. Machleidt, K. Holinde, and Ch. Elster, Phys. Rep. **149**, 1 (1987).

[37] R. Machleidt, Adv. Nucl. Phys. **19**, 189 (1989).

[38] M. R. Anastasio, L. S. Celenza, W. S. Pong, and C. M. Shakin, Phys. Rep. **100**, 327 (1983).

[39] B. ter Haar and R. Malfliet, Phys. Rep. **149**, 207 (1987).

[40] R. Brockmann and R. Machleidt, Phys. Rev. C **42**, 1965 (1990).

[41] G. Q. Li, R. Machleidt and R. Brockmann, Phys. Rev. C **45**, 2782 (1992).

[42] R. J. Furnstahl, D. K. Griegel, and T. D. Cohen, Phys. Rev. C **46**, 1507 (1992).

[43] X. Jin, T. D. Cohen, R. J. Furnstahl, and D. K. Griegel, Phys. Rev. C **47**, 2882 (1993).

[44] X. Jin, M. Nielsen, T. D. Cohen, R. J. Furnstahl, and D. K. Griegel, Phys. Rev. C **49**, 464 (1994).

[45] X. S. Fang, C. M. Ko, G. Q. Li, and Y. M. Zheng, Phys. Rev. C **49**, R608 (1994); Nucl. Phys. **A575**, 766 (1994).

[46] G. Q. Li and C. M. Ko, Phys. Lett. **B349**, 405 (1995).

[47] G. Q. Li and C. M. Ko, Nucl. Phys. **A594**, 439 (1995).

[48] E. Grosse, Prog. Part. Nucl. Phys. **30**, 89 (1993); P.Senger *et al.,* Nucl. Phys. **A553**, 757c (1993); D. Miskowiec, *et al.,* Phys. Rev. Lett. **72**, 3650 (1994).

[49] G. Q. Li, C. M. Ko, and X. S. Fang, Phys. Lett. **B329**, 149 (1994).

[50] A. Schröter, *et al.,* Nucl. Phys. **A553**, (1993) 775c; Z. Phys. A **350**, 101 (1994).

[51] G. Q. Li, C. M. Ko, X. S. Fang, and Y. M. Zheng, Phys. Rev. C **49**, 1139 (1994).

[52] G. Q. Li and C. M. Ko, Phys. Rev. C **50**, 1725 (1994).

[53] L. Xiong, C. M. Ko, and V. Koch, Phys. Rev. C **47**, 788 (1993).

[54] G. Odyniec *et al.,* in *Proc. of the 8th High Energy Heavy-Ion Study*, ed. J. Harris and G. Woznick, LBL Report No. 24580, p. 218 (1988).

[55] O. Schwalb *et al.,* Phys. Lett. **B321**, 20 (1994)

[56] G. Q. Li, C. M. Ko, and B. A. Li, Phys. Rev. Lett. **74**, 235 (1995); G. Q. Li and C. M. Ko, Nucl. Phys. **A594**, 460 (1995).

[57] J. Ritman and the FOPI collaboration, Z. Phys. **A352**, 355 (1995); D. Best, in *Advances in Nuclear Dynamics*, edited by W. Bauer *et al.,* (World Scientific, Singapore, 1996).

[58] G. Q. Li and C. M. Ko, Nucl. Phys. **A582**, 731 (1995).

[59] W. Koening, in *Proc. of Workshop on Dilepton Production in Relativistic Heavy-Ion Collisions*, ed. H. Bokemeyer, p. 225 (GSI, Darmstadt, 1994).

[60] C. M. Ko, Z. G. Wu, L. H. Xia, and G. E. Brown, Phys. Rev. Lett. **66**, 2577 (1991); G. E. Brown, C. M. Ko, Z. G. Wu, and L. H. Xia, Phys. Rev. C **43**, 1881 (1991).

[61] X. S. Fang, C. M. Ko, G. E. Brown, and V. Koch, Phys. Rev. C **47**, 1678 (1993).

[62] V. Koch, G. E. Brown, and C. M. Ko, Phys. Lett. **B265**, 29 (1991).

[63] T. Abbott, *et al.,* Phys. Rev. Lett. **64**, 847 (1990); **66**, 1567(1991).

[64] T. Abbott, *et al.,*, Phys. Rev. C **50**, 1024 (1994).

[65] G. Q. Li, C. M. Ko, and G. E. Brown, Phys. Rev. Lett. **75**, 4007 (1995); Nucl. Phys. **A606**, 568 (1996).

[66] G. Q. Li, C. M. Ko, G. E. Brown, and H. Sorge, Nucl. Phys. **A**, in press.

[67] G. Agakichiev *et al.*, Phys. Rev. Lett. **75**, (1995) 1272; J. P. Wurm for the CERES Collaboration, Nucl. Phys. **A590**, 103c (1995).

[68] M. Masera for the HELIOS-3 Collaboration, Nucl. Phys. **A590**, 93c (1995).

[69] I. Tserruya, Nucl. Phys. **A590**, 127c (1995).

[70] C. M. Ko and B. H. Sa, Phys. Lett. **B258**, 6 (1991).

[71] J. P. Guilland *et al.*, Nucl. Phys. **A525**, 499c (1991).

[72] C. M. Ko, M. Asakawa, and P. Lévai, Phys. Rev. C **46**, 1072 (1992).

[73] J. Bartke *et al.* (NA35 Collab.), Z. Phys. **C48**, 191 (1990); R. Stock *et al.* (NA35 Collab.), Nucl. Phys. **A525**, 221c (1990).

[74] C. DeTar and J. B. Kogut, Phys. Rev. D **36** (1987) 2828.

[75] T. Hashimoto, T. Nakamura, and I. O. Stamatescu, Nucl. Phys. **B406** (1993) 325.

[76] G. Boyd, S. Gupta, F. Karsch, E. Laermann, B. Petersson, and K. Redlich, Phys. Lett. B **349** (1995) 170.

[77] J. Boguta and A. R. Bodmer, Nucl. Phys. **A292**, 413 (1977).

[78] P.-G. Reinhard, Rep. Prog. Phys. **52**, 257 (1989).

[79] M. Jaminon and C. Mahaux, Phys. Rev. C **40**, 354 (1989).

[80] K. Saito, T. Maruyama, and K. Soutome, Phys. Rev. C **40**, 407 (1989).

[81] K. Soutome, T. Maruyama, and K. Saito, Nucl. Phys. **A507**, 731 (1990).

[82] R. J. Furnstahl and B. D. Serot, Phys. Rev. C **41**, 262 (1990).

[83] S. Klimt, M. Lutz, and W. Weise, Phys. Lett. B **249**, 386 (1990).

[84] T. Hatsuda, H. Hogaasen, and M. Prakash, Phys. Rev. C **42**, 2212 (1990).

[85] C. Adami and G. E. Brown, Z. Phys. A **340**, 93 (1991).

[86] M. A. Shifman, A. I. Vainshtein, and V. I. Zakharov, Nucl. Phys. **B147**, 385, 448, 519 (1979).

[87] B. L. Ioff, Nucl. Phys. **B188**, 317 (1981).

[88] L. J. Reinders, H. R. Rubinstein, and S. Yazaki, Phys. Rep. **127**, 1 (1985).

[89] M. A. Shifman, *Vacuum Structure and QCD Sum Rules* (North Holland, Amsterdam, 1992).

[90] L. Ray, G. W. Hoffmann, and W. R. Coker, Phys. Rep. **212**, 223 (1992).

[91] L. G. Arnold, B. C. Clark, and R. L. Mercer, Phys. Rev C **19**, 917 (1979); S. Hama, B. C. Clark, E. D. Cooper, H. S. Sherif, and R. L. Mercer, Phys. Rev. C **41**, 2737 (1990); E. D. Cooper, S. Hama, B. C. Clark, and R. L. Mercer, Phys. Rev. C **47**, 297 (1993).

[92] A. M. Kobos, E. D. Cooper, J. I. Johansson, and H. S. Sherif, Nucl. Phys. **A445**, 605 (1985).

[93] J. A. McNeil, J. R. Shepard, and S. J. Wallace, Phys. Rev. Lett. **50**, 1493 (1983); S. J. Wallace, Ann. Rev. Nucl. Part. Sci. **37**, 267 (1987).

[94] D. P. Murdock and C. J. Horowitz, Phys. Rev. C **35**, 1442 (1987).

[95] G. Q. Li, R. Machleidt, R. Fritz, H. Müther, and Y. Z. Zhuo, Phys. Rev. C **48**, 2443 (1993); G. Q. Li and Y. Z. Zhuo,

Nucl. Phys. **A568**, 745 (1994).

[96] M. Hoffman, R. Mattiello, H. Sorge, H. Stöcker, and W. Greiner, Phys. Rev. C **51**, 2095 (1995).

[97] B. A. Li and C. M. Ko, Phys. Rev. C **52**, 2037 (1995).

[98] C. M. Chen, D. J. Ernst, and M. B. Johnson, Phys. Rev. C **47**, R9 (1993).

[99] X. Jin, Phys. Rev. C **51**, 2260 (1995).

[100] D. J. Millener, C. B. Dover, and A. Gal, Phys. Rev. C **38** (1988) 2700; Y.Yamamoto, H. Bando, and J. Zofka, Prog. Theor. Phys. **80**, 757 (1988); B. F. Gibson and E. V. Hungerford III, Phys. Rep. **257**, 349 (1995).

[101] J. Schaffner, C. Greiner, and H. Stöcker, Phys. Rev. C **46**, 322 (1992).

[102] A. Reuber, K. Holinde, and J. Speth, Nucl. Phys. **A570**, 543 (1994).

[103] R. Brockmann and W. Weise, Phys. Lett. B **69**, 167 (1977).

[104] A. Bouyssy, Nucl. Phys. **A290**, 324 (1977).

[105] M. Rufa, J. Schaffner, J. Maruhn, H. Stöcker, W. Greiner, and P. G. Reinhard, Phys. Rev. C **42**, 2469 (1990).

[106] N. K. Glendenning and S. A. Moszkowski, Phys. Rev. Lett. **67** (1991) 2424; N. K. Glendenning, D. Van-Eiff, M. Haft, and H. Lenske, M. K. Weigel, Phys. Rev. C **48**, 889 (1993).

[107] X. Jin and M. Nielsen, Phys. Rev. C **51**, 347 (1995).

[108] X. Jin and R. J. Furnstahl, Phys. Rev. C **49**, 1190 (1994).

[109] V. Bernard, N. Kaiser, T.-S. H. Lee, and Ulf-G. Meissner, Phys. Rev. Lett. **70**, 387 (1993); Phys. Rep. **246**, 315 (1994).

[110] G. E. Brown, C. H. Lee, M. Rho, and V. Thorsson, Nucl. Phys. **A567**, 937 (1994).

[111] C. H. Lee, H. Jung, D. P. Min, and M. Rho, Phys. Lett. **B326**, 14 (1994).

[112] C. H. Lee, G. E. Brown, D. P. Min, and M. Rho, Nucl. Phys. **A585**, 401 (1995).

[113] T. Ericson and W. Weise, *Pions and Nuclei* (Clarendon Press, Oxford, 1988).

[114] G. E. Brown and W. Weise, Phys. Rep. **22**, 279 (1975).

[115] B. Friemann, V. P. Pandharipande, and Q. N. Usmani, Nucl. Phys. **A372**, 483 (1981).

[116] C. M. Ko, L. H. Xia, and P. J. Siemens, Phys. Lett. **B231**, 16 (1989).

[117] G. E. Brown, M. Vicent Vacas, and W. Weise, Nucl. Phys. **A505**, 823 (1989).

[118] L. H. Xia, P. J. Siemens, and M. Soyeur, Nucl. Phys. **A578**, 493 (1994).

[119] P. A. Henning and H. Umezawa, Nucl. Phys. **A571**, 617 (1994).

[120] C. L. Korpa and R. Malfliet, Phys. Rev. C **52**, 2756 (1995).

[121] G. E. Brown, V. Koch, and M. Rho, Nucl. Phys. **A535**, 701 (1991).

[122] V. Thorsson and A. Wirzba, Nucl. Phys. **A589**, 633 (1995).

[123] J. Delorme, M. Ericson, and T. E. O. Ericson, Phys. Lett. **B291**, 379 (1992).

[124] V. Bernard and U. G. Meissner, Nucl. Phys. **A489**, 647 (1988).

[125] M. Lutz, S. Klimt, and W. Weise, Nucl. Phys. **A542**, 521 (1992).

[126] C. Song, Phys. Lett. **B329**, 312 (1994).

[127] J. Rafelski and B. Müller, Phys. Rev. Lett. **48**, 1066 (1982); **56**, 2334 (E) (1986).

[128] G. E. Brown, K. Kubodera, D. Page, and P. Pizzecherro, Phys. Rev. D **37**, 2042 (1988).

[129] G. E. Brown and H. A. Bethe, Astrophys. Jour. **423**, 659 (1994).

[130] D. B. Kaplan and A. E. Nelson, Phys. Lett. **B175**, 57 (1986); A. E. Nelson and D. B. Kaplan, Phys. Lett. **B192**, 193 (1987).

[131] G. E. Brown, K. Kubodera, and M. Rho, Phys. Lett. **B192**, 273 (1987).

[132] H. D. Politzer and M. B. Wise, Phys. Lett. **B273**, 156 (1991).

[133] M. Lutz, A. Steiner, and W. Weise, Phys. Lett. **B278**, 29 (1992); Nucl. Phys. **A574**, 755 (1994).

[134] B. W. Lynn, A. E. Nelson, and N. Tetradis, Nucl. Phys. **B345**, 186 (1990).

[135] T. Muto and T. Tatsumi, Phys. Lett. **B283**, 165 (1992).

[136] G. E. Brown, C. M. Ko, and K. Kubodera, Z. Phys. A **341**, 301 (1992).

[137] H. Yabu, S. Nakamura, F. Myhrer, and K. Kubodera, Phys. Lett. **B315**, 17 (1993).

[138] J. Schaffer, A. Gal, I. N. Mishustin, H. Stöcker, and W. Greiner, Phys. Lett. **B334**, 268 (1994).

[139] B. W. Lynn, Nucl.Phys. **B402**, 281 (1993).

[140] S. J. Dong and K. F. Liu, Nucl. Phys. **B42** (Proc. Suppl.), 322 (1995).

[141] M. Fukugita, Y. Kuramashi, M. Okawa, and A. Ukawa, Phys. Rev. D **51**, 5319 (1995).

[142] R. K. Bhaduri, *Models of the Nucleon* (Addison-Wesley, Reading, MA, 1988).

[143] E. Shuryak and V. Thorsson, Nucl. Phys. **A536**, 739 (1992).

[144] G. E. Brown, C. M. Ko, and G. Q. Li, Nucl. Phys. **A**, submitted.

[145] G. Q. Li, C. M. Ko, and G. E. Brown, Phys. Lett. **B381**, 17 (1996).

[146] T. Maruyama, H. Fujii, T. Muto, and T. Tatsumi, Phys. Lett. B **337**, 19 (1994).

[147] H. Fujii, T. Maruyama, and T. Tatsumi, Nucl. Phys. **A597**, 645 (1996).

[148] R. Knorren, M. Prakash, and P. J. Ellis, Phys. Rev. C **52**, 3470 (1995).

[149] V. R. Pandharipande, C. J. Pethick, and V. Thorsson, Phys. Rev. Lett. **75**, 4638 (1995).

[150] A. D. Martin, Nucl. Phys. **B179**, 33 (1981).

[151] E. Friedman, A. Gal, and C. J. Batty, Phys. Lett. B **308**, 6 (1993); Nucl. Phys. **A579**, 518 (1994).

[152] N. Kaiser, P. B. Siegel, and W. Weise, Nucl. Phys. **A594**, 325 (1995).

[153] T. Waas, N. Kaiser, and W. Weise, Phys. Lett. B **365**, 12 (1996); B **379**, 34 (1996).

[154] R. Brockmann, W. Weise, and L. Tauscher, Nucl. Phys. **A308**, 365 (1978).

[155] M. Mizoguchi, S. Hirenzaki, and H. Toki, Nucl. Phys. **A567**, 893 (1994).

[156] V. Koch, Phys. Lett. B **337**, 7 (1994).

[157] C. H. Lee, D. P. Min, and M. Rho, Nucl. Phys. **A602**, 334 (1996).

[158] G. E. Brown and M. Rho, Phys. Rev. Lett. **66**, 2720 (1991).

[159] C. Adami and G. E. Brown, Phys. Rep. **224**, 1 (1993).

[160] H. C. Jean, J. Piekarewicz, and A. G. Williams, Phys. Rev. C **49**, 1981 (1994).

[161] H. Shiomo and T. Hatsuda, Phys. Lett. **B334**, 281 (1994).

[162] C. S. Song, P. W. Xia, and C. M. Ko, Phys. Rev. C **52**, 408 (1995).

[163] K. Saito and A. W. Thomas, Phys. Lett. **B327**, 9 (1994); Phys. Rev. C **51**, 1757 (1995).

[164] M. Asakawa and C. M. Ko, Nucl. Phys. **A572**, 732 (1994).

[165] A. Bhattacharyya, S. K. Ghosh, and S. C. Phatak, and S. Raha, nucl-th/9602042.

[166] C. Song, Phys. Lett. **B388**, 141 (1996).

[167] M. Asakawa and C. M. Ko, Nucl. Phys. **A560**, 399 (1993).

[168] M. Asakawa, C. M. Ko, P. Levai, and X. J. Qiu, Phys. Rev. C **46**, R1159 (1992).

[169] M. Herrmann, B. L. Friman, and W. Nörenberg, Nucl. Phys. **A560**, 411 (1993).

[170] T. Cohen, Phys. Rev. C **45**, 833 (1995).

[171] G. E. Brown and M. Rho, Phys. Lett. **B222**, 324 (1989).

[172] G. E. Brown, C. B. Dover, P. B. Siegel, and W. Weise, Phys. Rev. Lett. **60**, 2723 (1988).

[173] C. M. Chen and D. J. Ernst, Phys. Rev. C **45**, 2019 (1992).

[174] P. Bonche, Phys. Rev. C **13**, 1226 (1976).

[175] R. Y. Cusson, J. A. Maruhn, and H. W. Meldner, Phys. Rev. C **18**, 35 (1979).

[176] K. T. R. Davies and S. E. Koonin, Phys. Rev. C **23**, 2042 (1981).

[177] J. W. Negele, Rev. Mod. Phys. **54**, 739 (1985).

[178] R. Y. Cusson, P. G. Reinhard, H. Stöcker, M. R. Strayer, and W. Greiner, Phys. Rev. Lett. **55**, 2786 (1985).

[179] Y. Yariv and Z. Fraenkel, Phys. Rev. C **20**, 445 (1979); C **24**, 488 (1981).

[180] J. Cugnon, Phys. Rev. C **22**, 1885 (1980); J. Cugnon, D. Kinet, and J. Vandermeulen, Nucl. Phys. **A379**, 553 (1982).

[181] Y. Pang, T. J. Schlagel, and S. H. Kahana, Phys. Rev. Lett. **68**, 1743 (1992); **69**, 3290 (1993).

[182] H. Sorge, H. Stöcker, and W. Greiner, Ann. Phys. **192**, 266 (1989); R. Mattiello, H. Sorge, H. Stöcker, and W. Greiner, Phys. Rev. Lett. **63**, 1549 (1989); H. Sorge, Phys. Rev. C **52**, 3291 (1995).

[183] C. Y. Wong and K. T. R. Davies, Phys. Rev. C **28**, 240 (1983).

[184] H. S. Köhler and B. S. Nilsson, Nucl. Phys. **A471**, 318 (1988).

[185] H. Tang, C. H. Dasso, H. Esbenson, R. A. Broglia, and A. Winther, Phys. Lett. B **101**, 10 (1981).

[186] G. F. Bertsch, H. Kruse, and S. Das Gupta, Phys. Rev. C **29**, 673 (1984).

[187] H. Kruse, B. V. Jacak, and H. Stöcker, Phys. Rev. Lett. **54**, 289 (1985).

[188] J. Molitoris and H. Stöcker, Phys. Rev. C **32**, 346 (1985).

[189] J. Aichelin and G. F. Bertsch, Phys. Rev. C **31**, 1730 (1985).

[190] Ch. Gregoire, B. Remaud, F. Sebille, L. Vinet, and Y. Raffray, Nucl. Phys. **A465**, 317 (1987).

[191] R. J. Lenk and V. R. Pandharipande, Phys. Rev. C **39**, 2442 (1989).

[192] C. Y. Wong, Phys. Rev. C **25**, 1461 (1982).

[193] J. Aichelin and H. Stöcker, Phys. Lett. B **176**, 14 (1986).

[194] D. H. Boal and J. N. Glosli, Phys. Rev. C **38**, 1870 (1988).

[195] H. Feldmeier, Nucl. Phys. **A515**, 147 (1990).

[196] T. Maruyama, A. Ohnishi, and H. Horiuchi, Phys. Rev. C **42**, 386 (1990).

[197] A. Ono, H. Horiuchi, T. Maruyama, and A. Ohnishi, Phys. Rev. Lett. **68**, 2898 (1992).

[198] J. Cugnon, T. Mitutani, and J. Vandermeullen, Nucl. Phys. **A352**, 505 (1981).

[199] C. Gale, G. Bertsch, and S. Das Gupta, Phys. Rev. C **35**, 1666 (1987).

[200] J. Aichelin, A. Rosenhauer, G. Peilert, H. Stöcker, and W. Greiner, Phys. Rev. Lett. **58**, 1926 (1987).

[201] Q. B. Pan and P. Danielewicz, Phys. Rev. Lett. **70**, 2062 (1993).

[202] J. Zhang, S. Das Gupta, and C. Gale, Phys. Rev. C **50**, 1617 (1994).

[203] A. Bohnet, N. Ohtsuka, J. Aichelin, R. Linden, and A. Faessler, Nucl. Phys. **A494**, 349 (1989).

[204] A. Faessler, Nucl. Phys. **A495**, 103c (1989).

[205] R. K. Puri, N. Ohtsuka, E. Lehmann, A. Faessler, M. A. Martin, D. T. Khoa, G. Batko, and S. W. Huang, Nucl. Phys. **A575**, 733 (1994).

[206] T. Maruyama, S. W. Huang, N. Ohtsuka, G. Q. Li, A. Faessler, and J. Aichelin, Nucl. Phys. **A534**, 720 (1991); T. Maruyama, G. Q. Li, and A. Faessler, Phys. Lett. B **268**, 160 (1991).

[207] M. Cubero, M. Schönhofen, B. L. Friman, and W. Nörenberg, Nucl. Phys. **A519**, 345c (1990).

[208] M. Schönhofen, M. Cubero, B. L. Friman, W. Nörenberg, and Gy. Wolf, Nucl. Phys. **A572**, 112 (1994).

[209] S. J. Wang, B. A. Li, W. Bauer, and J. Randrup, Ann. Phys. **209**, 251 (1991).

[210] S. Mrowczynski and U. Heinz, Ann. Phys. **229**, 1 (1994).

[211] P. Danielewicz, Ann. Phys. **152**, 239 (1984).

[212] L. P. Kadanoff and G. Baym, *Quantum Statistical Mechanics* (Benjamin, New York, 1962).

[213] Q. Li and C. M. Ko, Mod. Phys. Lett. **3**, 465 (1988).

[214] P. Danielewicz and G. F. Bertsch, Nucl. Phys. **A533**, 712 (1991).

[215] Y. Kitazoe, M. Sano, H. Toki, and S. Nagamiya, Phys. Lett. **B166**, 35 (1986).

[216] D. E. Kahana, D. Keane, Y. Pang, T. Schlagel, and S. Wang, Phys. Rev. Lett. **74**, 4404 (1995).

[217] P. Danielewicz and S. Pratt, Phys. Rev. C **53**, 249 (1996).

[218] L. Xiong, Z. G. Wu, C. M. Ko, and J. Q. Wu, Nucl. Phys. **A512**, 772 (1990).

[219] Gy. Wolf, G. Batko, T. S. Biro, W. Cassing, and U. Mosel, Nucl. Phys. **A517**, 615 (1990).

[220] B. A. Li and W. Bauer, Phys. Rev. C **44**, 450 (1991).

[221] J. Randrup and C. M. Ko, Nucl. Phys. **A343**, 519 (1980); **A411**, 537 (1983).

[222] J. Aichelin and C. M. Ko, Phys. Rev. Lett. **55**, 2661 (1985).

[223] C. Dover and G. E. Walker, Phys. Rep. **89**, 1 (1982).

[224] J. Cugnon and J. Vandermeulen, Ann. de Phys. **14**, 49 (1989).

[225] X. S. Fang, C. M. Ko, and Y. M. Zheng, Nucl. Phys. **A556**, 449 (1993).

[226] B. ter Haar and R. Malfliet, Phys. Rev. C **36**, 1611 (1987).

[227] G. Q. Li and R. Machleidt, Phys. Rev. C. **48**, 1702 (1993); C **49**, 566 (1994).

[228] E. Suetomi, N. Kishida, and H. Kadotani, Phys. Lett. B **333**, 22 (1994).

[229] R. R. Dubey, G. S. Khandelwal, F. A. Cucinotta, and J. W. Wilson, J. Phys. G **22**, 387 (1996).

[230] E. I. Tanaka, H. Horiuchi, and A. Ono, Kyoto University preprint KUNS 1364 (1996).

[231] G. F. Bertsch, G. E. Brown, V. Koch, and B. A. Li, Nucl. Phys. **A490**, 745 (1989).

[232] J. Q. Wu and C. M. Ko, Nucl. Phys. **A499**, 810 (1989).

[233] G. Mao, Z. Li, and Y. Zhou, Phys. Rev. C. **49**, 3137 (1994).

[234] G. Mao, Z. Li, Y. Zhou, and E. Zhao, Phys. Lett. **B378**, 5 (1996).

[235] D. Lohse, J. W. Durso, K. Holinde, and J. Speth, Phys. Lett. **B234**, 235 (1990); Nucl. Phys. **A516**, 513 (1990).

[236] V. N. Russkikh, V. D. Toneev, Yu. B. Ivanov, and K. K. Gudima, GSI-92-32 Preprint (1992).

[237] S. W. Huang, A. Faessler, G. Q. Li, R. K. Puri, E. Lehmann, M. A. Matin and D. T. Khoa, Phys. Lett. **B298**, 41 (1993).

[238] C. Hartnack, J. Jaenicke and J. Aichelin, Nucl. Phys. **A580**, 643 (1994)

[239] A. Lang, W. Cassing, U. Mosel, and K. Weber, Nucl. Phys. **A541**, 507 (1992); T. Maruyama, W. Cassing, U. Mosel, S. Teis, and K. Weber, Nucl. Phys. **A573**, 653 (1994).

[240] B. A. Li, Phys. Rev. C **50**, 2144 (1994),

[241] S. Teis, W. Cassing, T. Maruyama, and U. Mosel, Phys. Rev. C **50**, 388 (1994).

[242] G. Batko, A. Faessler, S. W. Huang, E. Lehmann, and R. K. Puri, J. Phys. G **20**, 461 (1994).

[243] C. Hartnack, J. Aichelin, H. Stöcker, and W. Greiner, NATO Advanced Study Institute on Hot and Dense Nuclear Matter, NATO ASI series, Series B: Physics **335**, 885 (1994).

[244] S. Nagamiya, *et al.,* Phys. Rev. C **40**, 640 (1989).

[245] J. B. Carroll, Nucl. Phys. **A488**, 203c (1988); A. Shor, *et al.,* Phys. Rev. Lett. **63**, 2192 (1989).

[246] J. Cugnon and R. M. Lombard, Nucl. Phys. **A422**, 635 (1984).

[247] B. Schürmann and W. Zwermann, Phys. Lett. **B183**, 31 (1987).

[248] G. Q. Li, S. W. Huang, T. Maruyama, Y. Lotfy, D. T. Khoa and A. Faessler, Nucl. Phys. **A537**, 645 (1992); G. Q. Li, A. Faessler and S. W. Huang, Prog. Part. Nucl. Phys. **31**, 159 (1993).

[249] L. Xiong, C. M. Ko, and J. Q. Wu, Phys. Rev. C **42**, 2231 (1990).

[250] G. Batko, J. Randrup, and T. Vetter, Nucl. Phys. **A536**, 786 (1992).

[251] J. M. Laget, Phys. Lett. **B259**, 24 (1991).

[252] G. Q. Li and R. Machleidt, Phys. Rev. C **48**, 2707 (1993).

[253] J. Randrup, Phys. Lett. **B99**, 9 (1981).

[254] W. Zwermann and B. Schürmann, Phys. Lett. **B145**, 315 (1984).

[255] S. W. Huang, G. Q. Li, T. Maruyama, and A. Faessler, Nucl. Phys. **A547**, 653 (1992).

[256] C. M. Ko, Phys. Rev. C **29**, 2169 (1984).

[257] C. M. Ko, Phys. Lett. **B120**, 294 (1983); **B138**, 361 (1984).

[258] H. W. Barz and H. Iwe, Phys. Lett. **B153**, 217 (1985).

[259] R. Baldi *et al.*, Phys. Lett. **B68**, 381 (1977).

[260] O. Benary, L. R. Price, and G. Alexander, Report No. UCRL-2000 NN, 1970, p. 112.

[261] Y. F. Wang, in *Proc. of Heavy-Ion Physics at the AGS*, MIT Report No. MITLNS-2158, p. 239 (1993), Y. Akiba *et al.*, Phys. Rev. Lett. **76**, 2021 (1996).

[262] W. S. Chung, G. Q. Li, and C. M. Ko, Phys. Lett. **B**, submitted.

[263] O. Chamberlain, *et al.,* Nuovo Cimento, **3**, 447 (1956).

[264] T. Elioff, *et al.,* Phys. Rev. **128**, 869 (1962).

[265] D. E. Dorfan, *et al.,* Phys. Rev. Lett. **14**, 995 (1965).

[266] A. A. Baldin *et al.,* JETP Lett. **48**, 137 (1988); Nucl. Phys. **A519**, 407c (1990).

[267] J. Chiba, *et al.,* Nucl. Phys. **A553**, 771c (1993).

[268] P. Danielewicz, Phys. Rev. C **42**, 1564 (1990).

[269] G. Batko, W. Cassing, U. Mosel, K. Niita, and Gy. Wolf, Phys. Lett. **B256**, 331 (1991).

[270] C. Spieles, M. Bleicher, A. Jahns, R. Mattiello, H. Sorge, H. Stöcker, and W. Greiner, Phys. Rev. C **53**, 2011 (1996).

[271] C. M. Ko and X. Ge, Phys. Lett. **B205**, 195 (1988); C. M. Ko and L. H. Xia, Phys. Rev. C **40**, R1118 (1989).

[272] W. A. Love *et al.*, Nucl. Phys. **A525**, 601c (1991).

[273] H. Strobele *et al.,* Z. Phys. C **38**, 89 (1988).

[274] K. S. Lee and U. Heinz, Z. Phys. C **43**, 425 (1989).

[275] J. Sollfrank, P. Koch, and U. Heinz, Phys. Lett. B **252**, 256 (1990).

[276] H. W. Barz, G. Bertsch, D. Kusnezov, and J. Schulz, Phys. Lett. B **254**, 332 (1991).

[277] G. E. Brown, J. Stachel, and G. M. Welke, Phys. Lett. B **253**, 19 (1991).

[278] M. Kataja and P. V. Ruuskanen, Phys. Lett. B **243**, 181 (1990).

[279] M. I. Gorenstein and S. N. Yang, Phys. Rev. C **44**, 2875 (1991).

[280] W. Ehehalt, W. Cassing, A. Engel, U. Mosel, and Gy. Wolf, Phys. Lett. **B298**, 31 (1993).

[281] E. V. Shuryak, Phys. Rev. D **42**, 1764 (1990); E. V. Shuryak, Nucl. Phys. **A533**, 761 (1991).

[282] E. Shuryak and V. Thorsson, Nucl. Phys. **A536**, 739 (1992).

[283] P. Danilewicz, Phys. Rev. C **51**, 716 (1995).

[284] F. D. Berg, *et al.,* Phys. Rev. Lett. **72**, (1994) 977.

[285] J. Helgesson and J. Randrup, Ann. Phys. **244**, 12 (1995).

[286] V. Koch and G. F Bertsch, Nucl. Phys. **A552**, 591 (1993).

[287] H. H. Gutbrod, A. M. Poskanzer, and H. G. Ritter, Rep. Prog. Phys. **52**, 1267 (1989).

[288] H. H. Gutbrod, K. H. Kampert, B. Kolb, A. M. Poskanzer, H. G. Ritter, R. Schicker, and H. R. Schmidt, Phys. Rev. C **42**, 640 (1990).

[289] E. Hjort, *et al.*, in *Advances in Nuclear Dynamics*, edited by B. Back, W. Bauer, and J. Harris, p. 63 (World Scientific, Singapore,1993); D. Keane, *et al.*, in *Proc. of the 9th High Energy Heavy-Ion Study*, LBL Report LBL-35984, p. 63 (1993); M. D. Partland *et al.* (EOS collaboration), Phys. Rev. Lett. **75**, 2100 (1995).

[290] P. Danielewicz and G. Odyniec, Phys. Lett. **B157**, 146 (1985).

[291] B. A. Li, W. Bauer, and G. F. Bertsch, Phys. Rev. C **44**, 2095 (1991).

[292] S. A. Bass, C. Hartnack, H. Stöcker, and W. Greiner, Phys. Rev. Lett. **71**, 1144 (1993).

[293] B. A. Li, Nucl. Phys. **A570**, 797 (1994).

[294] A. Jahns, C. Spieles, H. Sorge, H. Stöcker, and W. Greiner, Phys. Rev. Lett. **72**, 3464 (1994).

[295] H. M. Xu, Phys. Rev. Lett. **67**, 2769 (1991).

[296] D. Krofcheck, *et al.,* Phys. Rev. C **46**, 1416 (1992).

[297] H. B. Zhou, Z. X. Li, and Y. Z. Zhou, Phys. Lett. **B318**, 19 (1993).

[298] G. Q. Li and C. M. Ko, Phys. Rev. **C**, in press.

[299] J. Zipprich, C. Fuchs, E. Lehmann, L. Sehn, S. W. Huang, and A. Faessler, nucl-th/9606013.

[300] H. Sorge, R. Mattiello, A. Jahns, H. Stöcker, and W. Greiner, Phys. Lett. B **271**, 37 (1991).

[301] P. Braun-Munzinger, J. Stachel, J. P. Wessels, and N. Xu, Phys. Lett. **B333**, 33 (1995).

[302] J. Stachel, Nucl. Phys. **A566**, 183c (1994).

[303] S. Ahmad *et al.*, Phys. Rev. C **52**, R2289 (1995).

[304] G. E. Brown and M. Rho, Phys. Lett. **B338**, 301 (1994).

[305] P. W. Xia and C. M. Ko, unpublished.

[306] V. Koch, Phys. Lett. **B351**, 29 (1995); Nucl. Phys. **A590**, 531c (1995).

[307] G. Q. Li and C. M. Ko, Phys. Lett. **B351**, 37 (1995).

[308] J. Aichelin and K. Werner, Phys. Lett. **B300**, 158 (1993).

[309] H. Sorge, M. Berenguer, H. Stöcker, and W. Greiner, Phys. Lett. **B289**, 6 (1992).

[310] J. Schaffner, I. N. Mishustin, L. M. Satarov, H. Stöcker, and W. Greiner, Z. Phys. A **341**, 47 (1991).

[311] C. Gale and J. Kapusta, Phys. Rev. C **35**, 2107 (1987); C **38**, 2657 (1988).

[312] L. H. Xia, C. M. Ko, L. Xiong, and J. Q. Wu, Nucl. Phys. **A485**, 721 (1988).

[313] R. Pisarski, Phys. Lett. 110B, 155 (1982).

[314] V. Koch, in *Proceedings of Pittsburgh Workshop on Soft lepton Pair and Photon Production*, ed. J. A. Thompson, (Nova Science Publishers, New York, 1992), p. 251.

[315] F. Karsch, K. Redlich, and L. Turko, Z. Phys. C **60**, 519 (1993).

[316] T. Hatsuda, Y. Koike, and S. H. Lee, Nucl. Phys. **B394**, 221 (1993).

[317] E. V. Shuryak, Phys. Lett. **B78**, 150 (1978).

[318] S. A. Chin, Phys. Lett. **B119**, 51 (1982).

[319] K. Kajantie, J. Kapusta, L. McLerran, and A. Mekjian, Phys. Rev. D **34**, 2746 (1986).

[320] C. M. Ko and L. H. Xia, Phys. Rev. Lett. **62**, 1595 (1989).

[321] M. Asakawa, C. M. Ko, and P. Lévai, Phys. Rev. Lett. **70**, 398 (1993).

[322] G. Roche *et al.,* Phys. Rev. Lett. **61**, 1069 (1988); C. Naudet *et al.,* Phys. Rev. Lett. **62**, 2652 (1988).

[323] Gy. Wolf, G. Batko, T. S. Biro, W. Cassing, and U. Mosel, Nucl. Phys. **A512**, 772 (1990).

[324] Gy. Wolf, W. Cassing, and U. Mosel, Nucl. Phys. **A552**, 549 (1993).

[325] L. A. Winckelmann, H. Sorge, H. Stöcker, W. Greiner, Phys. Rev. C **51**, R9 (1995).

[326] M. Hoffman, *et al.*, Nucl. Phys. **A566**, 15c (1994).

[327] Z. Huang and X. N. Wang, Phys. Rev. D **53**, 5034 (1996).

[328] J. Kapusta, D. Kharzeev, and L. McLerran, Phys. Rev. D **53**, 5028 (1996).

[329] D. K. Srivastava, B. Sinha, and C. Gale, Phys. Rev. **53**, R567 (1996).

[330] K. Haglin, Phys. Rev. C **53**, R2606 (1996).

[331] W. Cassing, W. Ehehalt, C. M. Ko, Phys. Lett. **B363**, 35 (1995).

[332] W. Cassing, W. Ehehalt, I. Kralik, Phys. Lett. **B377**, 5 (1996).

[333] V. Koch and C. Song, Phys. Rev. C **54**, 1903 (1996).

[334] L. Xiong and E. Shuryak, Phys. Lett. **B333**, 316 (1994).

[335] C. Song, C. M. Ko, and C. Gale, Phys. Rev. D **50**, R1827 (1994).

[336] C. Gale and P. Lichard, Phys. Rev. D **49**, 3338 (1994).

[337] K. Haglin and C. Gale, Phys. Rev. D **52**, 6297 (1995).

[338] L. Xiong and E. Shuryak, Nucl. Phys. **A590**, 589c (1995).

[339] T. Matsui and H. Satz, Phys. Lett. **B178**, 416 (1986).

[340] NA38 Collaboration, C. Baglin *et al.*, Phys. Lett. **B220**, 471 (1989); *ibid.*, **272**, 449 (1991); NA38 Collaboration, M. C. Abreu *et al.*, Nucl. Phys. **A544**, 209c (1992).

[341] C. Gerschel and J. Hüfner, Phys. Lett. **B207**, 253 (1988); Nucl. Phys. **A544**, 513c (1992).

[342] R. Vogt, M. Prakash, P. Koch, and T. H. Hansson, Phys. Lett. **B207**, 263 (1988); R. Vogt, S. J. Brodsky, and P. Hoyer, Nucl. Phys. **B360**, 67 (1991); R. Vogt, Nucl. Phys. **A544**, 615c (1992).

[343] S. Gavin, Nucl. Phys. **A566**, 383c (1994).

[344] M. Asakawa and C. M. Ko, Phys. Lett. **B322**, 33 (1994); Nucl. Phys. **A566**, 447c (1994); Phys. Rev. C **50**, 3064 (1994).

[345] R. J. Furnstahl, T. Hatsuda, and S. H. Lee, Phys. Rev. C **42**, 1744 (1990).

[346] C. M. Ko and D. Seibert, Phys. Rev. C **49**, 2198 (1994); **50**, R559 (1994).

[347] K. Haglin, Nucl. Phys. **A584**, 719 (1995).

[348] A. Baldini *et al.,* Total cross sections for reaction of high energy particles, (Springer-Verlag, Heidelberg, 1988).

[349] C. Spieles, A. Jahns, H. Sorge, H. Stöcker, and W. Greiner, in *Proceedings of XXXII International Winter Meeting on Nuclear Physics*, Ricerca Scientifica ed Educazione Permanente, Supplemento **97**, 423 (1994).

[350] B. A. Li, C. M. Ko, and G. Q. Li, Phys. Rev. **C50**, R2675 (1994).

[351] C. Spieles, A. Jahns, H. Stöcker, and W. Greiner, Mod. Phys. Lett. **A27**, 2547 (1993).

[352] G. M. Welke and G. F. Bertsch, Phys. Rev. C **45**, 1403 (1992).

[353] G. Bertsch and P. Danielewicz, Phys. Lett. **B367**, 55 (1996).

[354] W. Ehehalt and W. Cassing, Nucl. Phys. **A602**, 449 (1996).

[355] K. Geiger and B. Müller, Nucl. Phys. **B369**, 600 (1992).

[356] H. Th. Elze and U. Heinz, Phys. Rep. **183**, 81 (1989).

[357] L. P. Csernai and J. I. Kapusta, Phys. Rev. Lett. **69**, 737 (1992).